arXiv:1407.2865v1 [hep-ex] 10 Jul 2014

Experimental study of rare charged pion decays

Dinko Počanić[1], Emil Frlež[1] and Andries van der Schaaf[2]

[1] Institute for Nuclear and Particle Physics and Department of Physics, University of Virginia, Charlottesville, VA 22904-4714, USA

[2] Physik-Institut, Universität Zürich, CH-8057 Zürich, Switzerland

E-mail: pocanic@virginia.edu

Abstract.

The combination of simple dynamics, small number of available decay channels, and extremely well controlled radiative and loop corrections, make charged pion decays a sensitive means for testing the underlying symmetries and the universality of weak fermion couplings, as well as for improving our understanding of pion structure and chiral dynamics. This paper reviews the current state of experimental study of the allowed rare decays of charged pions: (a) leptonic, $\pi^+ \to e^+\nu_e$, or π_{e2}, (b) radiative, $\pi^+ \to e^+\nu_e\gamma$, or $\pi_{e2\gamma}$, and $\pi^+ \to e^+\nu_e e^+e^-$, or π_{e2ee}, and (c) semileptonic, $\pi^+ \to \pi^0 e^+\nu$, or π_{e3}. Taken together, the combined data set presents an internally consistent picture that also agrees well with standard model predictions. The internal consistency is illustrated well by the π_{e2} branching ratio of $(R^{\pi}_{e/\mu})^{\rm PIBETA} = (1.2366\pm0.0064)\times10^{-4}$ extracted in this work from the PIBETA measurement of the π_{e3} decay and the current best value for the CKM matrix element V_{ud}. However, even after the great progress of the recent decades, experimental precision is lagging far behind that of the theoretical description for all above processes. We review the implications of the present state of knowledge and prospects for further improvement in the near term.

PACS numbers: 13.20Cz, 12.39.Fe, 11.30.Rd

Submitted to: *J. Phys. G: Nucl. Part. Phys.*

1. Introduction

Pi mesons hold a special place in both the weak and the strong interactions, and remain subjects of research interest ever since their discovery almost 70 years ago [1].

Historically, pion decay has provided an important testing ground for the weak interaction and radiative corrections from the earliest time of the development of modern particle theory. Decays of the charged pion proceed via the weak interaction, and therefore closely reflect its properties and dynamics. In particular, the suppression of the direct electronic decay of the pion ($\pi \to e\nu$, or π_{e2}), manifested in the failure of initial searches to observe it, led to an early examination of the nature of the weak interaction governing pion decay [2]. A low branching fraction of $\sim 1.3 \times 10^{-4}$ was predicted [3] even before the decay's discovery [5], as a direct consequence of the $V-A$ nature of the weak interaction, through helicity suppression of the right-handed state of the electron. Not only was this prediction confirmed by the early measurements [5–7], the size of the radiative corrections [8, 9] was soon proved correct as well [10, 11].

In more recent times pion decays have been theoretically described with extraordinary precision. Thanks to the underlying symmetries and the associated conservation laws, the more complicated and thus more uncertain hadronic processes are suppressed. If measured with precision comparable to that of their theoretical description, pion decays offer an outstanding, clean testing ground of universality of lepton and quark couplings. Any documented deviation from standard model expectations would indicate presence of dynamics not included in the SM, affecting pion decays through loop diagrams.

In the hadronic sector the pion plays the role of the long-range exchange particle in effective nucleon-nucleon Lagrangians. Just as importantly, the pion also plays the role of the pseudo-Goldstone boson in the breaking of chiral symmetry for hadrons [12, 13]. Whereas early formulations of the phenomenon were focusing on nucleons as the fundamental hadronic fermions, the concept remains valid in the quark picture. While a massless pion would suffice to account for the spontaneous chiral symmetry breaking, the nonzero pion mass [14, 15] can be related directly to the light quark masses within the framework of the explicit chiral symmetry breaking, particularly in chiral perturbation theory (ChPT) [16–19]. Although in principle the full theory of quantum chromodynamics (QCD) contains all of this physics, in practice QCD does not readily provide manageable calculations in the low energy, nonperturbative domain. The situation will improve in the near future as lattice QCD calculations continue to increase accuracy, reliability and reach. Thus, for a long time chiral perturbation theory and other similar effective Lagrangian approximate methods have provided the primary and the only practical systematic treatment of low energy hadronic processes based on QCD. Basic properties of the pion, such as its charge radius and form factors, are closely related to the constants of the chiral Lagrangian [20] and are thus fundamental to nonperturbative QCD calculations.

In the remainder of this work we review experimental studies of individual rare

decay modes of the charged pion in the order of descending branching fraction, with a focus on recent and ongoing experiments. It is worth noting that almost all measurements to date have studied the positive pion. Stopped π^- mesons are captured with high probability in target nuclei (and undergo strong interactions), leaving few, if any, pions to decay weakly. Hence, in practice π^- decays can only be studied in flight in vacuo, with typically a tiny fraction of the beam pions decaying in the apparatus, and the remaining pions escaping before decaying. Positive pions can be easily stopped in a designated target, with a small fraction lost through prompt hadronic reactions with matter required to stop the beam. The stopped π^+'s decay with an exponential time distribution governed by the 26 ns pion lifetime. The dominant decay mode is $\pi^+ \to \mu^+\nu_\mu$ ($\pi_{\mu 2}$) which will not be discussed here. The resulting 4.1 MeV muons are typically contained in the target and decay via the $\mu^+ \to e^+\nu_e\bar{\nu}_\mu$ process with $\tau_\mu \simeq 2.2\,\mu$s.

2. The electronic $\pi \to e\bar{\nu}$ decay (π_{e2})

2.1. Motivation: processes affecting electron-muon universality

The $\pi^- \to \ell\bar{\nu}_\ell$ (or, equivalently, $\pi^+ \to \bar{\ell}\nu_\ell$) decay connects a pseudoscalar 0^- state (the pion) to the vacuum. At the lowest, tree level, the ratio of the $\pi \to e\bar{\nu}$ to $\pi \to \mu\bar{\nu}$ decay widths is given by [3, 21]

$$R^\pi_{e/\mu,0} = \frac{\Gamma(\pi \to e\bar{\nu})}{\Gamma(\pi \to \mu\bar{\nu})} = \frac{m_e^2}{m_\mu^2} \cdot \frac{(m_\pi^2 - m_e^2)^2}{(m_\pi^2 - m_\mu^2)^2} \simeq 1.283 \times 10^{-4}\,. \tag{1}$$

The first factor in the above expression, the ratio of squared lepton masses for the two decays, comes from the helicity suppression by the $V-A$ lepton-W boson weak couplings. If, instead, the decay could proceed directly through the pseudoscalar current, the ratio $R^\pi_{e/\mu}$ would reduce to the second, phase-space factor, or approximately 5.5. More complete treatment of the process includes $\delta R^\pi_{e/\mu}$, the radiative and loop corrections, and the possibility of lepton universality violation, i.e., that g_e and g_μ, the electron and muon couplings to the W, respectively, may not be equal:

$$R^\pi_{e/\mu} = \frac{\Gamma(\pi \to e\bar{\nu}(\gamma))}{\Gamma(\pi \to \mu\bar{\nu}(\gamma))} = \frac{g_e^2}{g_\mu^2}\frac{m_e^2}{m_\mu^2}\frac{(m_\pi^2 - m_e^2)^2}{(m_\pi^2 - m_\mu^2)^2}\left(1 + \delta R^\pi_{e/\mu}\right)\,, \tag{2}$$

where the "(γ)" indicates that radiative decays are fully included in the branching fractions. Steady improvements of the theoretical description of the π_{e2} decay since the 1950's have recently culminated in a series of calculations that have refined the Standard Model (SM) prediction to a precision of 8 parts in 10^5:

$$\left(R^\pi_{e/\mu}\right)^{\rm SM} = \left.\frac{\Gamma(\pi \to e\bar{\nu}(\gamma))}{\Gamma(\pi \to \mu\bar{\nu}(\gamma))}\right|_{\rm calc} = \begin{cases} 1.2352(5) \times 10^{-4} & \text{Ref. [22]}, \\ 1.2354(2) \times 10^{-4} & \text{Ref. [23]}, \\ 1.2352(1) \times 10^{-4} & \text{Ref. [24]}. \end{cases} \tag{3}$$

A comparison with equation (1) reveals that the radiative and loop corrections amount to almost 4% of $R^\pi_{e/\mu}$. However, as discussed below, the experimental precision at this time lags behind the theoretical one by more than an order of magnitude.

Because of the large helicity suppression of the π_{e2} decay, its branching ratio is highly susceptible to small non-$V-A$ contributions from new physics, making this decay a particularly suitable subject of study, as discussed in, e.g., Refs. 25–30. This prospect provides the primary motivation for the ongoing PEN [31] and PiENu [32] experiments. Of the possible "new physics" contributions in the Lagrangian, π_{e2} is directly sensitive to the pseudoscalar one. At the precision of 10^{-3}, $R^{\pi}_{e/\mu}$ probes the pseudoscalar and axial vector mass scales up to 1,000 TeV and 20 TeV, respectively [29, 30]. For comparison, Cabibbo-Kobayashi-Maskawa (CKM) matrix unitarity and precise measurements of several superallowed nuclear beta decays constrain the non-SM vector contributions to > 20 TeV, and scalar to > 10 TeV [37]. Although scalar interactions do not directly contribute to $R^{\pi}_{e/\mu}$, they can do so through loop diagrams, resulting in sensitivity to new scalar interactions up to 60 TeV [29,30]. The subject was recently reviewed at length in Ref. [33]. In addition, $(R^{\pi}_{e/\mu})^{\rm exp}$ provides limits on masses of certain SUSY partners [28], and on neutrino sector anomalies [27].

2.2. Past measurements of the $\pi \to e\bar{\nu}$ decay branching ratio

Even though $R^{\pi}_{e/\mu}$ is small, of order 10^{-4}, it would be relatively straightforward to measure precisely because of the large difference in decay ejectile energies, 69.79 MeV vs. 4.12 MeV for the e and μ channels, respectively. However, the subsequent decay of the muon, $\mu \to e\bar{\nu}_e\nu_\mu$, with the endpoint energy of 52.83 MeV, effectively brings the two processes kinematically closer, making the clean identification of the direct $\pi \to e$ events challenging in a "tail" overlap region discussed below. This complication is partly mitigated by the ~ 85 times longer lifetime of the muon than that of the pion. Selecting only early decays, say, within a couple of pion lifetimes, suppresses the sequential $\pi \to \mu \to e$ events by more than an order of magnitude, thus effectively enhancing the apparent $\pi \to e\bar{\nu}$ branching ratio. Nearly all experiments to date have used a variant of the stopped pion decay technique to measure $R^{\pi}_{e/\mu}$.

The technique based on detecting and normalizing $\pi \to e$ to $\pi \to \mu \to e$ decays at rest in a nonmagnetic spectrometer is inherently independent of several important sources of systematic uncertainty that are shared by the two processes, and that consequently cancel in the ratio. Prime examples of shared uncertainties that cancel include the relative placement of the target and the positron detector and the resulting acceptance. (On the other hand, using a magnetic spectrometer removes this insensitivity, as it would introduce a strong dependence of the solid angle on e^+ momentum.) Further cancellations occur for the efficiency of positron detection (largely independent of E_{e^+}, although corrections at the 10^{-3}–10^{-2} level are typically needed), various beam properties, efficiency of pion stop identification in the target, overall trigger efficiency etc. All of these quantities would have to be determined with higher precision in an experiment that would normalize the detected π_{e2} decay events to the corresponding number of beam pions stopped in the target. Additional quantities such as the time displacement of the first detection interval from the arrival time of

the pion and duration of the detection time gate, affect the extraction of $R^{\pi}_{e/\mu}$ in well understood ways.

The first notable measurement of $R^{\pi}_{e/\mu}$ with 6% uncertainty (rather than an upper limit or detection of a small number of π_{e2} decay events), was performed by the University of Chicago group with positive pions stopped inside a double-focusing magnetic spectrometer [10]. This work was soon followed by a $\sim$ 2% measurement [11] at the Columbia Nevis synchrocyclotron laboratory; decay positrons from π^+'s stopped in an active target were detected in a $\varnothing 23\,\mathrm{cm} \times 24\,\mathrm{cm}$ NaI(Tl) detector. Given the NaI detector size and acceptance for photons, the analysis included low-E_γ inner bremsstrahlung (IB) radiative $\pi^+ \to e^+\nu_e\gamma$ events in the branching fraction, in accordance with the theoretical definition of $R^{\pi}_{e/\mu}$, as given in (2).

The Nevis measurement brought to light an important experimental uncertainty, related to how accurately the NaI(Tl) energy response function is known. Positrons in the few to a hundred MeV energy range generate electromagnetic showers that cannot be completely contained in a finite-sized physical detector volume; there is a non-zero probability that some energy will escape the volume, primarily in the form of photons, inducing a low-energy "tail" in the response function to a monoenergetic positron. (Use of a magnetic spectrometer would eliminate this problem, though at the cost of significantly more complicated acceptance systematics.) This intrinsic instrumental tail coexists with the physical "tail" of radiative decay events for which the accompanying photon escaped detection, primarily due to limited detector solid angle. We note in passing that in a nearly hermetic detector, radiative decays will generate a high energy "tail" extending above the $\sim$69.8 MeV two-body decay positron energy; this was not a feature of the early measurements. In a sufficiently segmented detector such events can be properly treated by analyzing $(E + pc)/2$ rather than E alone.

The tail correction for $\pi \to e\nu$ events falling below the μ decay endpoint energy in the Nevis experiment was 9.1% with a $\sim$0.7% combined systematic and statistical uncertainty. While this correction diminishes for larger detectors, especially with external active enclosures, it remains a dominant source of systematic uncertainty for $R^{\pi}_{e/\mu}$, especially as experiments approach the theoretical precision of equation (3).

The TRIUMF group of Bryman and collaborators [34] used a similar technique to that used in the Nevis measurement, with improvements. TINA, the TRIUMF NaI(Tl) detector was larger at $\varnothing 46\,\mathrm{cm} \times 51\,\mathrm{cm}$ long, and subtended a solid angle of $\simeq$ 0.7% of 4π sr, with energy resolution of about 4% full width at half-maximum (FWHM) at 70 MeV, almost four times better than the Nevis detector's $\sim$15%. The experiment collected approximately 3.2×10^4 π_{e2} decay events. The resulting branching ratio had a 1.2% overall uncertainty. The single largest contribution to the uncertainty, at 0.75%, arose from the tail correction.

TINA was used again in a follow-up measurement (figure 1) by the same group [35], with numerous improvements in experimental design including an increased solid angle coverage of 2.9% of 4π sr and an order of magnitude more detected π_{e2} decay events.

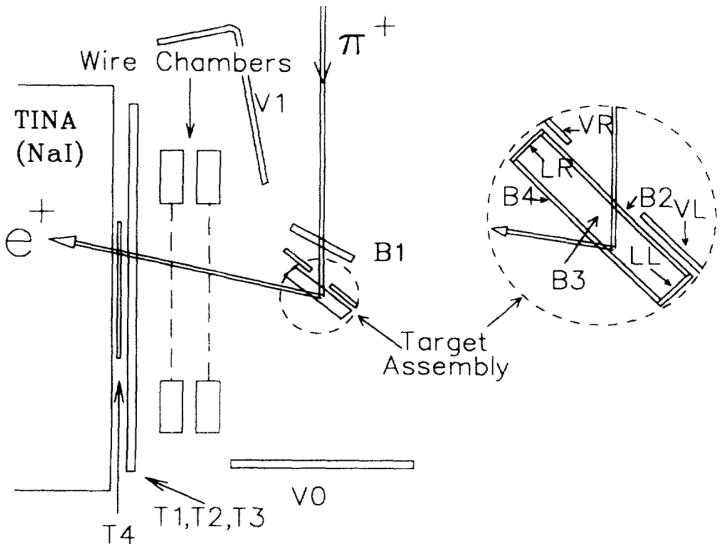

Figure 1. TRIUMF TINA experimental setup, with beam (B), veto (V), trigger (T) counters, and beam entering from top of page. For further details see [35].

The measured branching fraction

$$R^{\pi}_{e/\mu} = [1.2265 \pm 0.0034(\text{stat}) \pm 0.0044(\text{syst})] \times 10^{-4}\,, \tag{4}$$

is in excellent agreement with standard model predictions.

At the Paul Scherrer Institute (PSI) a Bern–PSI group performed a measurement of $R^{\pi}_{e/\mu}$ at a similar level of precision using a radically different apparatus [36], essentially simultaneously with the TRIUMF measurement. The Bern–PSI setup is shown in figure 2. The key component of the apparatus was a nearly hermetic $\sim 4\pi$ sr calorimeter

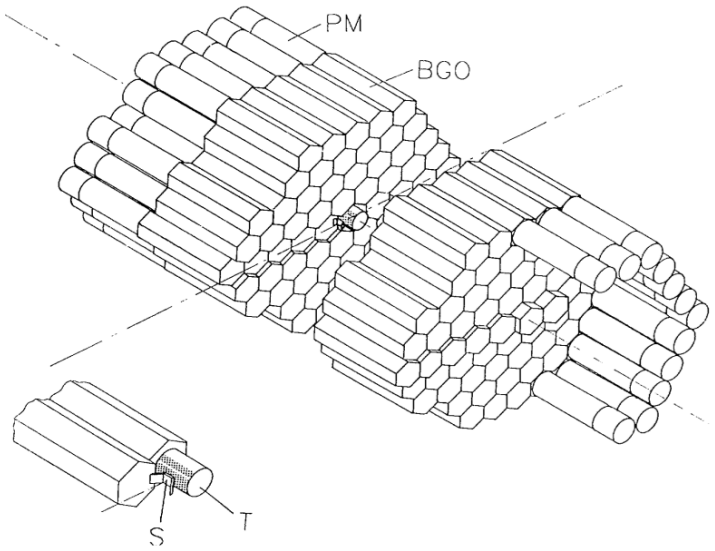

Figure 2. Bern-PSI BGO calorimeter apparatus, shown with the two BGO "walls" separated, and the closeup of the last beam defining scintillator (S) and active target (T) counters; the pion beam enters from the left. For further details see [36].

Table 1. Summary of published experimental results on $R^{\pi}_{e/\mu}$, and the Particle Data Group (PDG) average.

Experiment	π_{e2} events	$10^4 \cdot R^{\pi}_{e/\mu}$	Reference
U. Chicago/EFINS	1.2k	1.21 ± 0.07	[10]
Columbia/Nevis	10.8k	1.247 ± 0.028	[11]
TRIUMF/TINA	32k	1.218 ± 0.014	[34]
TRIUMF/TINA	190k	1.2265 ± 0.0056	[35]
Bern–PSI	120k	1.2346 ± 0.0050	[36]
PDG average	342k	1.230 ± 0.004	[37]

consisting of 132 bismuth germanium oxide (BGO) detectors in the shape of hexagonal prisms, each 20 cm or 18 radiation lengths long, and with inscribed radius of 5.5 cm. The detectors were arranged so that a narrow opening allowed the beam (almost equal parts pions and muons) to stop in a small cylindrical plastic scintillator (active target), whose light was read out by a central calorimeter crystal. The resulting rms resolution was sub-2% at 70 MeV. Because of the hermetic nature of the calorimeter, radiative muon decays presented a significant background under the $\pi \to e\bar{\nu}(\gamma)$ signal peak in the energy spectrum. A total of 3×10^5 $\pi \to e$, and 1.2×10^6 $\pi \to \mu$ events were recorded. The resulting branching fraction was

$$R^{\pi}_{e/\mu} = [1.2346 \pm 0.0035(\text{stat}) \pm 0.0036(\text{syst})] \times 10^{-4}\,,$$

with the systematic uncertainty coming primarily from corrections for photonuclear reactions, radiative μ decay background, and electromagnetic losses.

Table 1 summarizes the available experimental results on $R^{\pi}_{e/\mu}$. Combined, the 1992/93 TRIUMF and PSI results define the present experimental precision for the decay [37], as the earlier measurements do not significantly affect the current global average:

$$\left(R^{\pi}_{e/\mu}\right)^{\text{exp}} = (1.230 \pm 0.004) \times 10^{-4}\,. \tag{5}$$

This experimental world average lags behind the theoretical precision of (3) by more than an order of magnitude. The precision gap, already notable in 1993, has only increased with the passage of time, and has motivated a new generation of experiments currently under way, and briefly discussed below.

2.3. The PEN experiment at PSI

In 2006 a new measurement of $R^{\pi}_{e/\mu}$ was proposed at the Paul Scherrer Institute by a collaboration of seven institutions from the US and Europe [31], with the aim to reach

$$\frac{\Delta R^{\pi}_{e/\mu}}{R^{\pi}_{e/\mu}} \simeq 5 \times 10^{-4}\,. \tag{6}$$

The PEN experiment uses an upgraded version of the PIBETA detector system, described in detail in Ref. [38], and previously used in a series of rare pion and muon

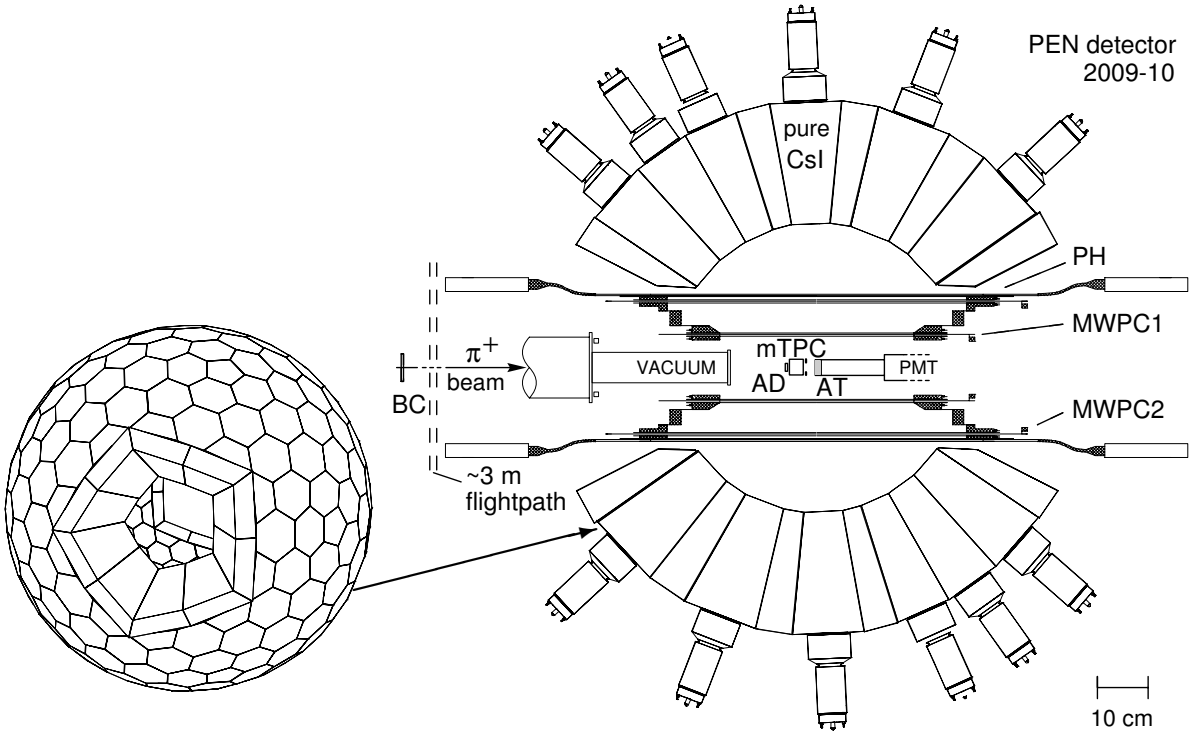

Figure 3. Schematic cross section of the PIBETA/PEN apparatus, shown in the 2009 PEN configuration, with its main components: beam entry with the upstream beam counter (BC), 5 mm thick active degrader (AD), mini time projection chamber (mTPC) followed by a passive Al collimator, and active target (AT), cylindrical multiwire proportional chambers (MWPC's), plastic hodoscope (PH) detectors and photomultiplier tubes (PMT's), 240-element pure CsI electromagnetic shower calorimeter and its PMT's. BC, AD, AT and PH detectors are made of plastic scintillator. For details concerning the detector performance see [38].

decay measurements [39–42]. The main component of the PEN apparatus, shown in figure 3, is a spherical large-acceptance ($\sim 3\pi$ sr) electromagnetic shower calorimeter. The calorimeter consists of 240 truncated hexagonal and pentagonal pyramids of pure CsI, 22 cm or 12 radiation lengths deep. The inner and outer diameters of the sphere are 52 cm and 96 cm, respectively. Beam particles entering the apparatus with $p \simeq 75\,\mathrm{MeV}/c$ are first tagged in a thin upstream beam counter (BC) and refocused by a triplet of quadrupole magnets. After a ~ 3 m long flight path they pass through a 5 mm thick active degrader (AD) and a low-mass mini time projection chamber (mTPC), finally to reach a 15 mm thick active target (AT) where the beam pions stop. Decay particles are tracked non-magnetically in a pair of concentric cylindrical multiwire proportional chambers (MWPC1,2) and an array of twenty 4 mm thick plastic hodoscope detectors (PH), all surrounding the active target. The BC, AD, AT and PH detectors are all made of fast plastic scintillator material and read out by fast photomultiplier tubes (PMTs). Signals from the beam detectors are sent to waveform digitizers, running at 2 GS/s for BC, AD, and AT, and at 250 MS/s for the mTPC.

As discussed in the preceding section, a key source of systematic uncertainty in previous π_{e2} experiments has been the hard to measure low energy tail of the detector response function, caused by electromagnetic shower leakage from the calorimeter, mostly in the form of photons. PEN is no exception in this respect. Other physical processes, if not properly identified and suppressed, also contribute events to the low energy part of the spectrum; unlike shower leakage they can also produce high energy events. One process is ordinary pion decay into a muon in flight, before the pion is stopped, with the resulting muon decaying within the time gate accepted in the measurement. Another is the unavoidable physical process of radiative decay. The latter is well measured and properly accounted for in the PEN apparatus, as discussed below in the section on radiative decay. Shower leakage and pion decays in flight can only be well characterized if the $\pi \to \mu \to e$ chain can be well separated from the direct $\pi \to e$ decay in the target. Therefore much effort has been devoted to digitization, filtering and analysis of the target waveforms [43], as illustrated in figure 4. The method used for separating the 2-peak (π_{e2}) and 3-peak ($\pi \to \mu \to e$) events is illustrated and explained in figure 5. The key to the method is provided by the beam and MWPC detectors which are used to predict the pion and positron energy deposition in the target, and the times of their signals. Once the predicted waveform is subtracted the net waveform is scanned for the presence of a 4.1 MeV muon peak. The difference between the minimum χ^2 values with and without the muon peak is reported as $\Delta(\chi^2)$, constructed so that clean 2-peak and 3-peak fits return values of $+1$ and -1, respectively. The scan is fast

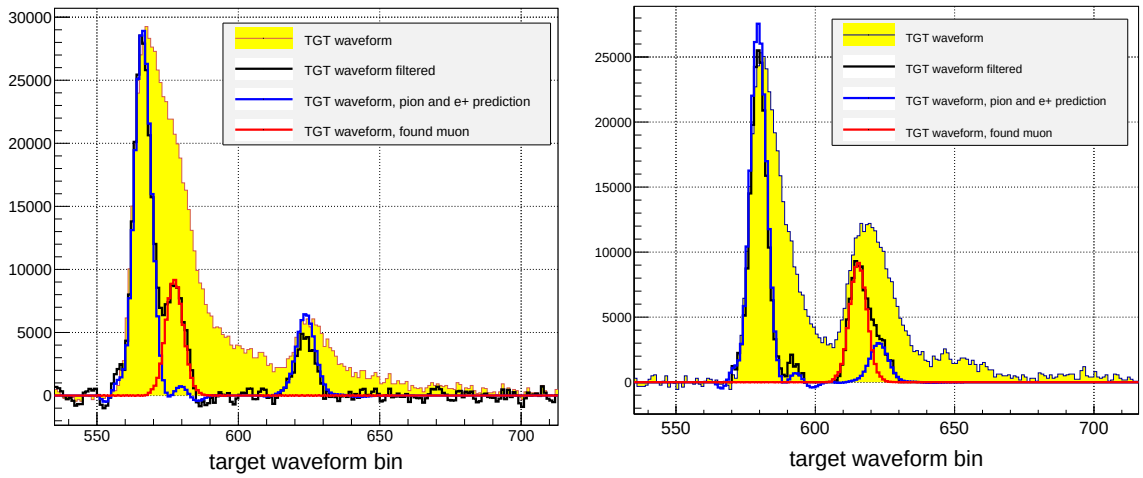

Figure 4. Full and filtered active target (TGT) waveform in the PEN experiment for two challenging $\pi \to \mu \to e$ sequential decay events with an early $\pi \to \mu$ decay (left) and early $\mu \to e$ decay (right). The filtering procedure consists of a simple algebraic manipulation of the signal. To the naked eye both raw waveforms appear to have two peaks only. The separation of events with/without a muon signal depends critically on the accuracy of the predictions for the pion and positron signals. For the pion the prediction is based on the times and energies observed in BC and AD. For the positron the prediction depends on PH timing and the pathlength reconstructed with the pion and positron tracking detectors (see figure 5).

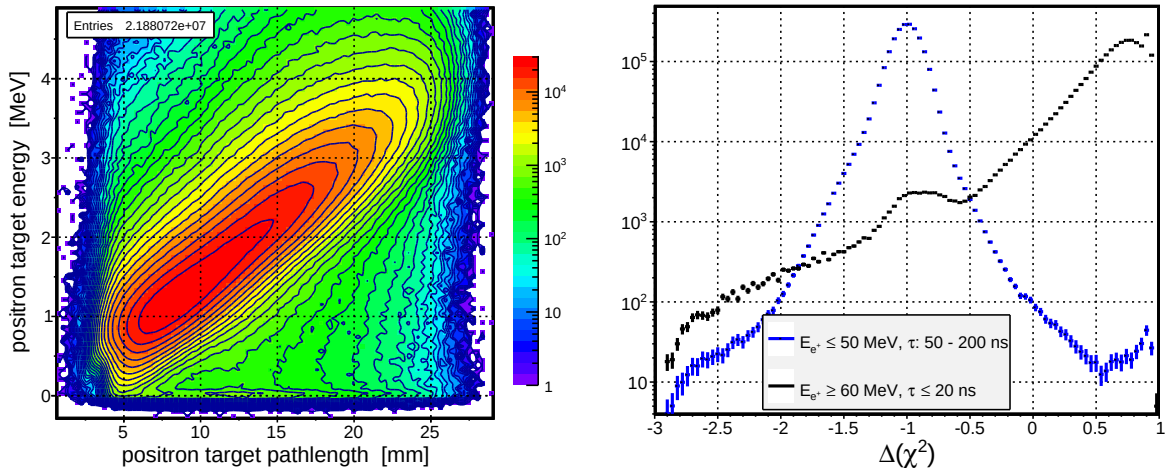

Figure 5. Left: correlation between observed positron energy in the target waveform and the e^+ path length in the target, reconstructed from the observed π^+ and e^+ trajectories. Shown are events with proper $\pi \to \mu \to e$ sequences for which the e^+ signal is well separated from other signals. Right: difference in χ^2 for the assumptions of a target waveform with/without a muon pulse present. The observable is normalized such that $\pi \to e\nu$ events peak at $+1$, and $\pi \to \mu \to e$ at -1. Shown are events for two different combinations of e^+ energy and decay time resulting in almost pure samples of $\pi \to e\nu$ and $\pi \to \mu \to e$, respectively. Tiny admixtures of another process are readily identified and are of great help in reducing the systematic uncertainties.

and returns a $\Delta(\chi^2)$ value for every event, as illustrated in the figure.

A particularly telling figure regarding the PEN data quality are the decay time histograms of the $\pi \to e\nu$ decay and $\pi \to \mu \to e$ sequence, shown in figure 6 for a subset of data recorded in 2010. The $\pi \to e\nu$ data follow the exponential decay law over more than three orders of magnitude, and perfectly predict the measured $\pi \to \mu \to e$ sequential decay data once the latter are corrected for random (pile-up) events. Both event ensembles were obtained with minimal requirements (cuts) on detector observables, none of which bias the selection in ways that would affect the branching ratio. The probability of random $\mu \to e$ events originating in the target can be controlled in the data sample by making use of multihit time to digital converter (TDC) data that record early pion stop signals. With this information one can strongly suppress events in which an "old" muon was present in the target by the time of the pion stop that triggered the readout.

The "intrinsic" low energy tail of the PEN response function below $\sim 50\,\mathrm{MeV}$, due to shower losses for π_{e2} decay events for pions at rest, amounts to approximately 2% of the full yield. Events with $\pi \to \mu$ decays in flight, with subsequent ordinary Michel decay of the stopped muon in the target, add a comparable contribution to the tail. The two contributions can be simulated accurately, with the respective detector responses independently verified through comparisons with measured data in appropriately selected processes and regions of phase space. These response functions are entered into the maximum likelihood analysis (MLA), used to describe all measured

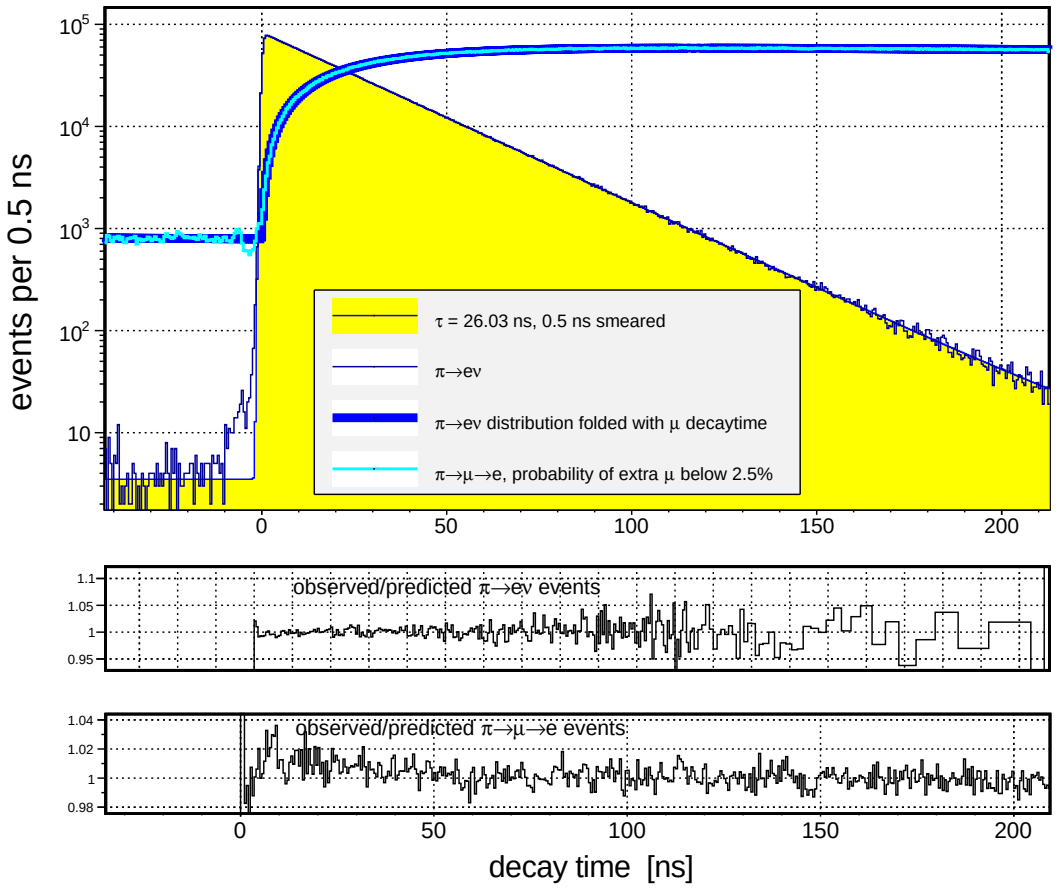

Figure 6. Decay time histograms for a subset of 2010 PEN data: $\pi \to e\nu$ events and $\pi \to \mu \to e$ sequential decay events. The two processes are distinguished primarily by the total e^+ energy and by the absence or presence, respectively, of an extra 4.1 MeV (muon) in the target due to $\pi \to \mu$ decay. The π_{e2} data are shown with a pion lifetime $\tau_\pi = 26.03$ ns exponential decay function superimposed. The $\pi \to \mu \to e$ data were prescaled by a factor of $\sim 1/64$; they are shown with the cut on the probability of $< 2.5\%$ for a second, pile-up muon to be present in the target at $t = 0$, the time of the nominal pion stop. The turquoise histogram gives the $\pi \to \mu \to e$ yield constructed entirely from the measured $\pi \to e\nu$ data folded with the μ decay rate, and corrected for random muons; it perfectly matches the bold dark blue histogram. The two lower plots show the observed to predicted ratios for π_{e2} and $\pi \to \mu \to e$ events, respectively. The scatter in the ratio plots is statistical in nature.

processes simultaneously. The quantity $R^\pi_{e/\mu}$ is evaluated in the MLA as the ratio of the magnitudes found for the $\pi \to e(\gamma)$ and $\pi \to \mu \to e$ processes. Although verified through comparisons with Monte Carlo simulations, the intrinsic tail itself is not directly measurable at the required precision because of the statistical uncertainties arising in the tail data selection procedure. Radiative decay processes are directly measurable and accounted for in the MLA procedure. More information about the PEN/PIBETA detector response functions is given below, in the section on π_{e3} decays, and in [38].

During the 2008-10 production runs the PEN experiment accumulated some 2.3×10^7 $\pi \to e\nu$, and more than 1.5×10^8 $\pi \to \mu \to e$ events, as well as significant

numbers of pion and muon radiative decays. A comprehensive blinded maximum likelihood analysis is under way to extract a new experimental value of $R^{\pi}_{e/\mu}$. As of this writing, there appear no obstacles that would prevent the PEN collaboration to reach a precision of $\Delta R/R < 10^{-3}$. The competing PiENu experiment at TRIUMF, discussed below, has a similar precision goal. The near to medium future will thus bring about a substantial improvement in the limits on e-μ lepton universality, and the attendant SM limits.

2.4. The PiENu experiment at TRIUMF

The new PIENU experiment at TRIUMF builds on the earlier measurements at the same laboratory [35], aiming at a significant improvement in precision through refinements of the technique used. The branching fraction will again be obtained from the ratio of positron yields from the $\pi \to e\nu$ decay and from the $\pi \to \mu \to e$ decay chain. As in other experiments that detect decay positrons in a nonmagnetic spectrometer, many normalization factors, such as the solid angle of positron detection, cancel to first order in PiENu, leaving only corrections for small energy-dependent effects. Major improvements in precision in PiENu over the earlier TRIUMF TINA measurement derive from improved geometry and beamline, a superior calorimeter, as well as high-speed digitizing of all detector signals.

Figure 7 shows a schematic rendition of the PiENu experimental apparatus. A 75 MeV/c π^+ beam from the improved TRIUMF M13 beam line [44] is tracked in wire chambers, identified by plastic scintillators, and stopped in a 0.8 cm thick scintillator target. Fine tracking near the target is provided by two sets of single-sided silicon strip detectors located immediately upstream and downstream of the target assembly. The positrons from $\pi \to e\nu$ and $\pi \to \mu \to e$ decays are detected in the positron telescope, which consists of a silicon strip counter, two thin plastic counters, and an acceptance-defining wire chamber that covers the front of the crystal calorimeter. The solid-angle acceptance of the telescope counters is 20% of 4π sr.

The primary energy measurement is performed using BINA, a cylindrical, single-crystal $\varnothing$48 cm $\times$ 48 cm long NaI(Tl) detector [45]. BINA's energy resolution of approximately 2.2% FWHM for incident positrons at 70 MeV [46] is better by a factor of approximately two than the resolution observed in the previous measurement with TINA [35]. The NaI detector is surrounded by two layers consisting of 97 pure CsI crystals, 8.5 cm thick and 2$\times$25 cm long [47, 48] to capture electromagnetic shower leakage from BINA, thus helping to suppress the instrumental low-energy "tail".

As in PEN, analog signals from plastic scintillators, silicon strip, NaI, and CsI detectors are recorded as waveforms, using appropriately fast digitizers. To suppress background arising from old muon decay signals in the target region and to reduce possible distortions in the time spectrum due to pileup, the incident pion rate is kept at 6×10^4/s.

The PiENu collaboration has accumulated upwards of 2×10^7 $\pi \to e\nu$ events through

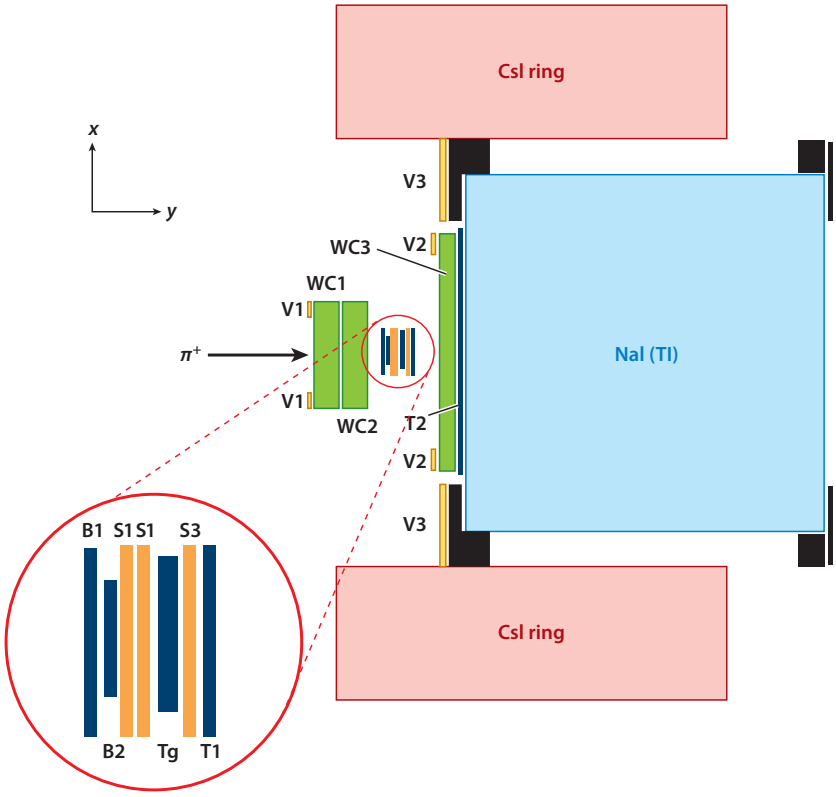

Figure 7. The TRIUMF PiENu experiment setup [32]. The beam enters from the left. "B" and "T" refer to the beam pion and positron telescope plastic scintillation counters, respectively. For more details see [32, 33, 44, 46].

2012. Combining the corresponding statistical uncertainty with reduced systematic uncertainties, the collaboration expects to reach $\Delta R^{\pi}_{e/\mu}/R^{\pi}_{e/\mu} < 0.1\%$. The data acquisition phase of the experiment indeed ended in 2012, and, as of this writing, the collaboration is working on data analysis.

3. Radiative decays $\pi \to e\nu\gamma$ ($\pi_{e2\gamma}$) and $\pi \to e\nu\gamma e^+e^-$ (π_{e2ee})

3.1. General considerations

The decay $\pi^+ \to e^+\nu_e\gamma$ proceeds via a combination of QED (inner bremsstrahlung, IB) and direct, structure-dependent (SD) amplitudes [20,21]. Under normal circumstances, as in $\pi \to \mu\nu\gamma$ decay, the direct amplitudes are hopelessly buried under an overwhelming inner bremsstrahlung background. However, the strong helicity suppression of the primary non-radiative process, $\pi \to e\nu$, also suppresses the bremsstrahlung terms, making the direct structure dependent amplitudes measurable in certain regions of phase space [20, 49]. (We recall that the same helicity suppression made possible sensitive searches for non-$V-A$ interaction terms in precision measurements of the primary $\pi \to e\nu$ decay, discussed in section 2.) This result is of great use to effective low-energy theories of the strong interaction, primarily ChPT, which rely on the SD amplitudes to

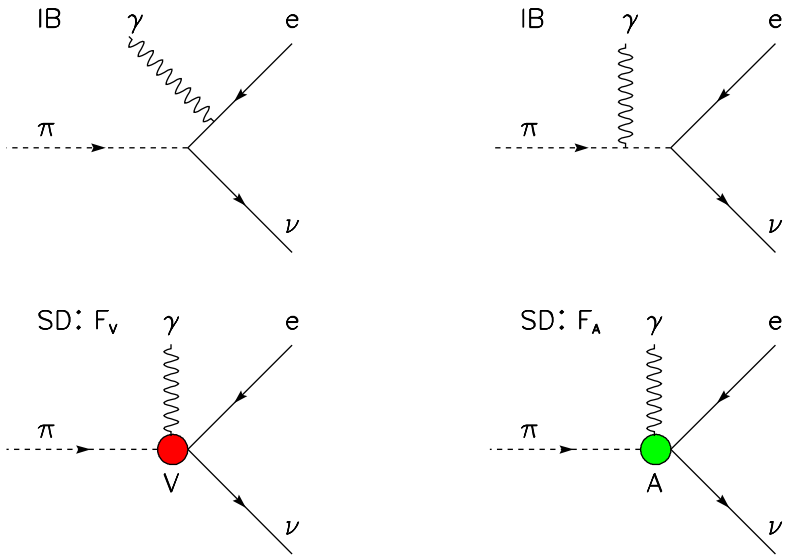

Figure 8. Tree-level diagrams of the inner bremsstrahlung (IB) and structure-dependent (SD) amplitudes determined by the vector and axial-vector form factors, F_V and F_A, respectively. A new interaction type, such as one mediated by a hypothetical tensor particle proposed and discussed in the literature through the 1990s, would add an SD amplitude defined by a corresponding form factor, i.e., F_T.

provide important input parameters. Whereas the IB amplitude is completely described by QED, the structure-dependent amplitude can be parametrized in terms of the pion form factors. As indicated in the tree-level Feynman diagrams in figure 8, standard $V-A$ electroweak theory requires only two pion form factors, F_A, axial vector, and F_V, vector (or polar-vector), to describe the SD amplitude. The amplitudes (form factors) F_A and F_V in principle depend on the 4-momentum transfer to the e-ν pair (or to the W boson), $s = (p_e + p_\nu)^2 \equiv q^2$. In $\pi \to e\nu\gamma$ decay s remains low, $s < m_\pi^2$, so that it is a good approximation to evaluate F_V and F_A at $s = 0$, often referred to as the soft pion limit. It is useful at this point to consider the tree-level double differential branching ratio for the $\pi \to e\nu\gamma$ decay which, in the usual parametrization, takes the form first worked out in detail by De Baenst and Pestieau [50]:

$$\frac{\mathrm{d}^2\Gamma_{\pi e2\gamma}}{\mathrm{d}x\,\mathrm{d}y} = \frac{\alpha}{2\pi}\Gamma_{\pi e2}\left\{ IB\,(x,y) + \left(\frac{F_V m_\pi^2}{2 f_\pi m_e}\right)^2 \left[(1+\gamma)^2\, SD^+(x,y) + (1-\gamma)^2\, SD^-\,(x,y)\right] \right.$$
$$\left. + \left(\frac{F_V m_\pi}{f_\pi}\right)\left[(1+\gamma)\, S^+_{\mathrm{int}}\,(x,y) + (1-\gamma)\, S^-_{\mathrm{int}}\,(x,y)\right]\right\}, \qquad (7)$$

where $x \equiv 2E_\gamma/m_\pi$ and $y \equiv 2E_e/m_\pi$ are the appropriately normalized photon and electron (positron) energies, respectively, $\gamma \equiv F_A/F_V$ is the ratio of the axial and the vector pion form factors, f_π is the familiar pion decay constant and "int" denotes interference terms between the IB and SD amplitudes. The functional dependence of the terms IB, SD^+, SD^- SD^+_{int} and SD^-_{int} on x and y is well established and is given in

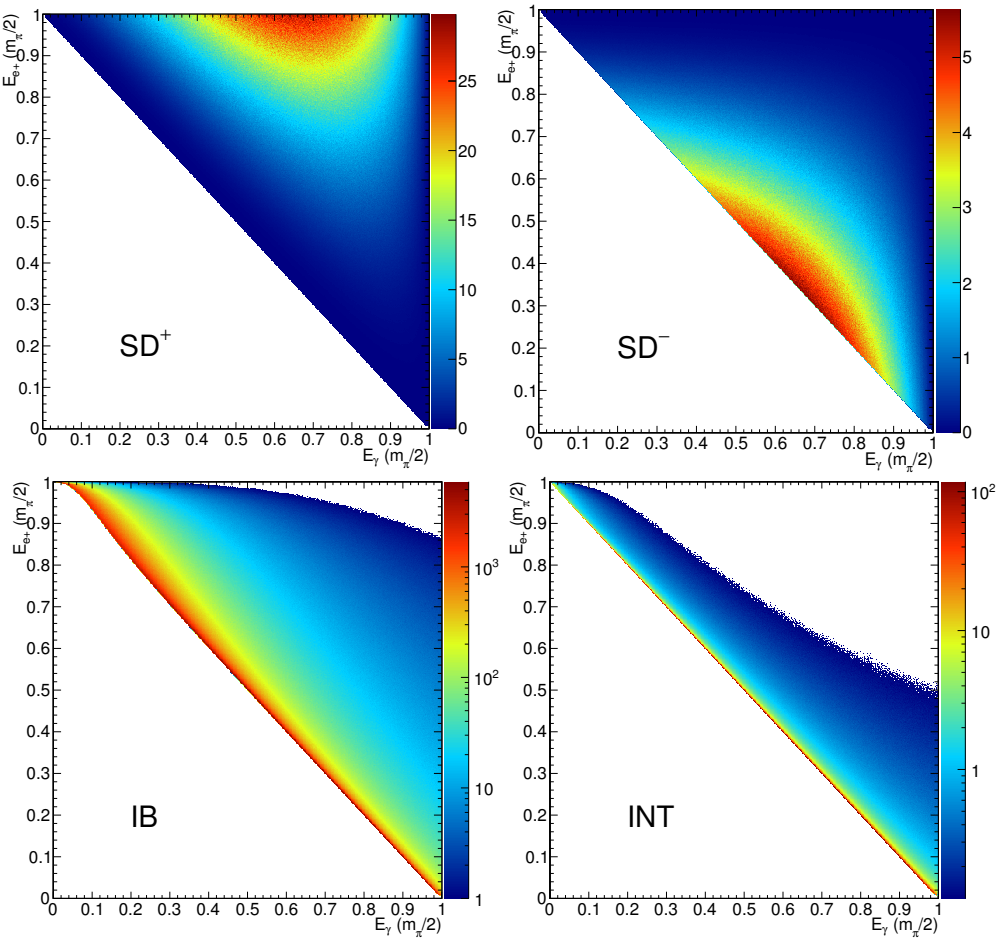

Figure 9. Relative strengths of the physics amplitudes in $\pi \to e\nu\gamma$ decay: structure-dependent amplitudes SD^+ and SD^-, inner bremsstrahlung IB, and interference $INT \propto (1+\gamma)S^+_{\rm int} + (1-\gamma)S^-_{\rm int}$, plotted as functions of E_γ and E_e.

the literature, e.g., in [21, 50]. We note that the SD^+ and SD^- terms, which multiply the $(F_V + F_A)^2$ and $(F_V - F_A)^2$ form factor terms, respectively, map very different portions of the 3-body phase space in the final state. The SD^+ term peaks for large values of positron energies, $y \gtrsim 0.9$ and moderate photon energies, $x \gtrsim 0.5$, where there is relatively little background from the IB terms. The SD^- term, on the other hand, peaks for low values of $x + y \simeq 1$, where the IB amplitude is comparatively strong, as shown in figure 9; this kinematic region is also susceptible to background from muon radiative decays. It is not surprising, then, that most of the measurements of the $\pi_{e2\gamma}$ decay to date have focused on determining the SD^+ amplitude.

The conserved vector current (CVC) hypothesis [3, 4] relates the vector form factor F_V to the $\pi^0 \to \gamma\gamma$ decay amplitude [51–53]:

$$\Gamma_{\pi^0\to\gamma\gamma} = \frac{1}{2}\pi m_\pi \alpha^2 \left|F_V\right|^2 . \tag{8}$$

During a long period of time ending in 2012, then current Particle Data Group values for the π^0 lifetime and the $\pi^0 \to \gamma\gamma$ branching fraction led to a CVC prediction of $F_V^{\rm CVC} = 0.0259 \pm 0.0009$. As a rule, radiative pion decay measurements had access only

to one structure dependent amplitude, the SD^+. Treating the value of F_V as known, predicted by the CVC hypothesis, allowed analyses of $\pi_{e2\gamma}$ data to extract F_A, or, more specifically the ratio $\gamma \equiv F_A/F_V$. Recent measurements of the π^0 lifetime, primarily that of the PrimEx collaboration [54], have led to a change in the PDG accepted value of the pion lifetime, along with a reduced uncertainty. Furthermore, Bernstein and Holstein have recently pointed out the necessary correction to the CVC expression in (8) arising from isospin breaking effects [49]. Combined, the two effects lead to a new isospin corrected CVC prediction for the pion vector form factor:

$$F_V^{\mathrm{CVC}} = 0.0255 \pm 0.0003\,, \tag{9}$$

which modifies the previously reported values for F_A or $\gamma \equiv F_A/F_V$.

Before discussing individual measurements of the radiative $\pi^+ \to e^+\nu_e\gamma$ decay, we note that the related decay $\pi^+ \to e^+\nu_e e^+e^-$, where the photon is virtual, adds R, a second axial vector amplitude or form factor, to the SD terms. The R form factor is proportional to $\langle r_\pi^2\rangle$, the electromagnetic (charge) radius of the pion squared [20].

3.2. Measurements prior to the year 2000

3.2.1. Ordinary radiative decay $\pi_{e2\gamma}$. The first determination of the SD amplitudes in $\pi_{e2\gamma}$ decay was performed by Depommier and collaborators. In their apparatus pions were stopped in a plastic scintillator target, and the decay positrons and photons detected in opposing NaI(Tl) and lead glass detectors, each preceded by a pair of thin plastic scintillator detectors in front [55]. Signals from all detectors were recorded on oscilloscope pictures which were subsequently analyzed. A total of 148 ± 15 $\pi_{e2\gamma}$ events resulted after background subtraction; some 110 were due to the SD emission. In their analysis, the authors used $F_V = 0.0245$ and obtained two solutions for γ, 0.4 and -2.1; the data did not favor one over the other. The authors also reported a branching ratio for $E_e, E_\gamma > 48\,\mathrm{MeV}$ with 17% relative uncertainty, where, however, the detector resolution had not been taken into account, so the result could not be compared with theoretical calculations.

The Berkeley-UCLA experiment by Stetz and collaborators [56] detected the positrons in a magnetic spectrometer and the photons in a lead glass Čerenkov hodoscope. The experimenters observed 226 ± 22.4 events, and reported a branching ratio of $(5.6 \pm 0.7) \times 10^{-8}$ for $E_e > 56\,\mathrm{MeV}$ and $\theta_{e\gamma} > 132^\circ$. To determine the SD terms, the authors used $F_V = 0.0261 \pm 0.0009$, based on the 1977 average value for the π^0 lifetime. They, too, found two solutions for γ: 0.44 ± 0.12 or -2.36 ± 0.12, neither of which was clearly favored by the data.

In the mid-1980's at the Swiss Institute for Nuclear Research (SIN, now part of PSI) a Lausanne–Zurich collaboration [57] set up an improved version of the Berkeley-UCLA apparatus to study the $\pi_{e2\gamma}$ decay and determine F_A. They used an intense pion beam with the stopping rate in the target of $2.5 \times 10^7\,\mathrm{s}^{-1}$, an 8×8 array of NaI(Tl) crystals for photon detection, and a large-acceptance magnetic spectrometer for the positron. An MWPC near the target provided additional tracking information. Data were taken in

two detector geometries, centered around $\theta_{e\gamma} = 180°$ and 135°, respectively. The former configuration accepts negligible contributions from the IB and SD^- amplitudes, while the latter accepts a sizable SD^- contribution still with minimal IB background. Using this method, the collaborators collected 653 ± 29 $\pi_{e2\gamma}$ events, as well as 801 ± 34 π_{e2} events for normalization. Thanks to the expanded phase space coverage compared to previous experiments, Bay *et al* were able to resolve the quadratic ambiguity inherent in the SD^+ analysis only, and eliminate the negative-sign solution by a confidence factor of 8.5. Using the CVC value of $F_A = 0.0255(5)$, incidentally the same central value as the current best isospin-corrected CVC prediction in (9), the authors obtained $\gamma = 0.52 \pm 0.06$, or $F_A = 0.0133 \pm 0.0015$.

Around the same time as the SIN experiment, a group at the Los Alamos Meson Physics Facility (LAMPF) made a measurement of F_A/F_V [58] using the Crystal Box detector which consisted of 396 NaI(Tl) crystals, 36 plastic scintillation hodoscope counters, and a cylindrical drift chamber surrounding the stopping target [59]. Unlike the other experiments discussed above, the Crystal Box detector's single-particle acceptance for events originating in the target was about 45% of 4π sr. Such a large acceptance enabled the experimenters to cover a broad portion of the decay phase space, collecting 2364 coincidence events that included both decay signals and random coincidences. However, only 71 ± 11 high-energy nearly back-to-back photon-positron pairs were used to determine γ, as they were largely background free and strongly dominated by the SD^+ amplitude. The low statistics is reflected in the large relative uncertainty in $\gamma = 0.25 \pm 0.12$; however the remaining ∼2300 coincident events were included in a maximum likelihood analysis which preferred the positive γ solution by a factor of 2175:1. In all, the likelihood analysis found a total of 179 ± 18 $\pi \to e\nu\gamma$ events, in good agreement with the integral of the e-γ timing peak. Thus, although a low statistics measurement, this experiment's main result is the strongly favored selection of the $\gamma > 0$ solution, removing the prior longstanding quadratic ambiguity.

Although the subject of this review are measurements of rare decays of the pion, it is worthwhile to consider the 1988 analysis of Dominguez and Solà [60] who extracted a soft-pion value for $F_A(0)$ from semileptonic tau lepton decays, $\tau \to \nu_\tau + n\pi$. Analysis of decays with odd (even) values of n gives access to the vector (axial-vector) hadronic spectral functions up to the kinematical limit $t \sim 3\,\mathrm{GeV}^2$. Dominguez and Solà studied and refined such fits to existing τ decay data, and extracted the soft-pion value of $F_A(0) = 0.017 \pm 0.004$, or $\gamma(0) = F_A(0)/F_V(0) = 0.67 \pm 0.17$, with $F_V^{\mathrm{CVC}} \simeq 0.0254$. We note that this result is *independent of pion radiative decay* data.

The lone measurement of $\pi \to e\nu\gamma$ decays in flight was performed by the Moscow Institute for Nuclear Research (INR) group, using the ISTRA apparatus and a 17 GeV pion beam at the IHEP Protvino U70 accelerator [61]. The experimental technique and systematics are radically different from all of the stopped pion decay measurements discussed so far. Since decays occurred in flight, the experimenters were free to use negative pions and observe $\pi^- \to e^-\nu\gamma$ decays, making this the only experiment to date to do so. The wide acceptance of the apparatus enabled the experimenters to study the

pion rest frame kinematical region defined by

$$E_\gamma > 21\,\mathrm{MeV}, \quad E_e > 70\,\mathrm{MeV} - 0.8E_\gamma, \quad \text{and} \quad \theta_{e\gamma} > 60^\circ\,. \tag{10}$$

The results of this work, obtained in a maximum likelihood analysis, can be summarized as follows: (a) $\gamma \equiv F_A/F_V = 0.41 \pm 0.23$ (with no corresponding value for F_V quoted explicitly), (b) negative solution for γ disfavored by a likelihood factor of 5×10^9 or 6.7 standard deviations, (c) an independently determined $F_V = 0.014 \pm 0.009$, and (d) the branching ratio for the kinematic limits of equation (10), $B = (1.61 \pm 0.23) \times 10^{-7}$. Although not explicitly given, the total number of $\pi \to e\nu\gamma$ decay events appears to be approximately 90 after background subtraction, which would explain the large quoted uncertainties. Besides the strong preference for the $\gamma > 0$ solution, this work presented another notable result: a deficit of SD^- events, forcing a non-physical negative SD^- amplitude. The authors speculated that the deficit may be due to a destructive interference with a tensor term of the size $F_T = 0.0056 \pm 0.0017$. We will revisit the tensor hypothesis below.

3.2.2. The decay $\pi^+ \to e^+\nu_e e^+ e^-$ (or π_{e2ee}) merits special mention, as it contributes information not accessible through the regular $\pi_{e2\gamma}$ radiative decay channel. Following unsuccessful attempts [62], the π_{e2ee} decay was first observed by the SINDRUM I collaboration in a 1985 experiment [63]; the same data were reanalyzed more carefully and the results reported in 1989 [64].

The SINDRUM detector system, which became known as "SINDRUM I" after the construction of "SINDRUM II", was built primarily to search for the forbidden $\mu \to 3e$ decay [65]. The instrument, schematically depicted in figure 10, was capable of recording the trajectories of electrons and positrons in a solenoidal magnetic field with the help of five concentric cylindrical MWPC's of very similar design and construction to those used later in the PIBETA/PEN experiments. Decay particles were required to reach a 64 element scintillating hodoscope situated outside the tracking detectors, resulting in a lower threshold on transverse momentum around $17\,\mathrm{MeV}/c$. A cone-shaped 12-element segmented scintillating target was used, enabling a reduction of random coincidences between beam pions and decay particles by an order of magnitude.

In their first paper Egli *et al* [63] reported merely the first observation of the decay, with 79 recorded events. The authors also reported values of form factor ratios $\gamma = F_A/F_V$ and R/F_V with large uncertainty limits. They were, however, able to exclude by a ratio of 9:1 the previously reported large negative value of $\gamma = -2.49 \pm 0.06$ from $\pi_{e2\gamma}$ [56] in favor of a smaller positive solution $\gamma = 0.7 \pm 0.5$, thus anticipating the soon to follow $\pi_{e2\gamma}$ results of the Lausanne–Zurich [57] and LAMPF [58] groups.

In a second article [64], the SINDRUM I collaboration reported results of a more careful and comprehensive analysis of the same 1985 data set. By applying a series of cuts designed to reduce the backgrounds, the authors arrived at a data set of 98 events with 1 background event, based on $\sim 4 \times 10^{12}$ pions stopped in the target. Using this event set, the detector acceptance, the CVC value $F_V = 0.0255$, the Bay *et al*

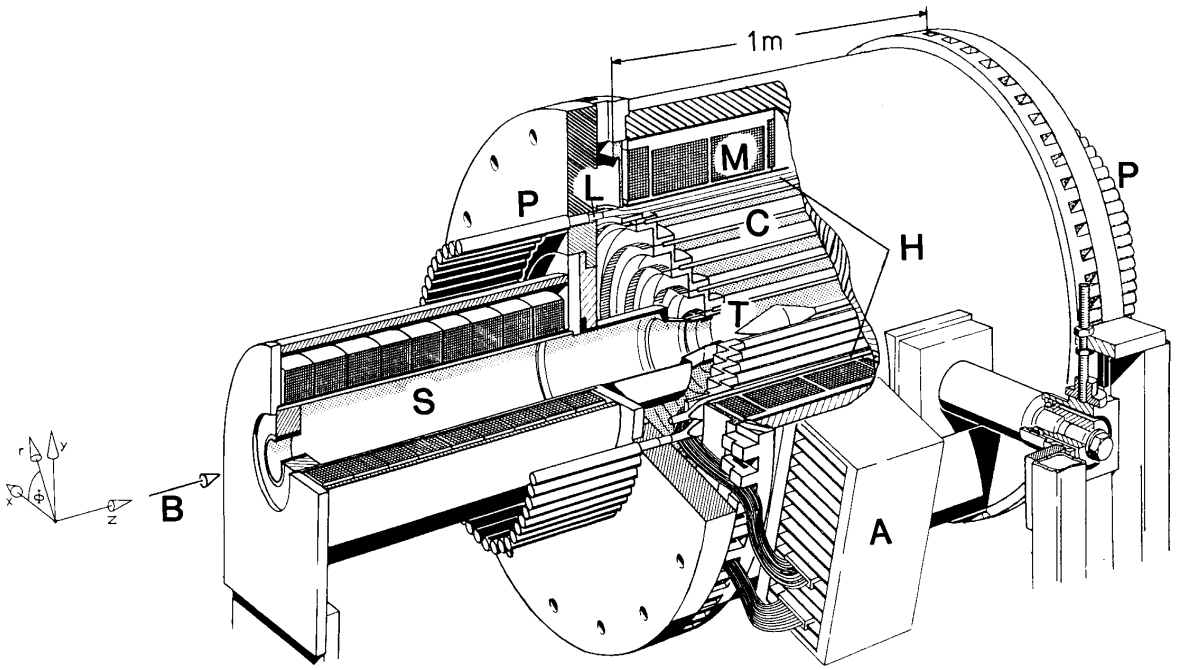

Figure 10. Schematic view of the SINDRUM I spectrometer as originally configured for the $\mu \to eee$ search [65]: B, μ beam; S, focusing solenoid (not used with the pion beam); T, target (a different target was used for the π_{e2ee} measurement); C, five cylindrical MWPC's; H, hodoscope of 64 scintillators; L, light guides for the hodoscope; P, 128 photomultiplier tubes; A, cathode strip preamplifiers and anode wire amplifier/discriminators; M, magnet coil. For further details see [63–65]

value $F_A = 0.0133 \pm 0.015$ [57] and the PCAC value for the second axial form factor $R_{\rm PCAC} = 0.068 \pm 0.004$, the authors derive the branching ratio for the full phase space:

$$B(\pi^+ \to e^+\nu_e e^+ e^-) = (3.2 \pm 0.5 \pm 0.2) \times 10^{-9}\,, \tag{11}$$

where the second uncertainty is propagated from $R_{\rm PCAC}$. Of additional interest are the values for the three pion form factors derived in a likelihood analysis of the data:

$$F_V = 0.023^{+0.015}_{-0.013}\,, \qquad F_A = 0.021^{+0.011}_{-0.013}\,, \qquad R = 0.059^{+0.009}_{-0.008}\,. \tag{12}$$

It is worth noting that fixing the vector form factor value to $F_V^{\rm CVC} = 0.0255$ does not significantly alter the maximum likelihood values of F_A and R.

A subsequent Dubna experiment [66] which detected only 7 events of π_{e2ee} decay did not improve the precision of the SINDRUM I branching ratio for the decay.

3.2.3. Summary of the early measurements: The $\pi^+ \to e^+\nu_e\gamma$ and $\pi^+ \to e^+\nu_e e^+e^-$ results published prior to 2000 may be summarized as follows.

(i) The positive-sign solution for $\gamma \equiv F_A/F_V$ was established with high likelihood by three experiments, effectively ruling out a negative solution.

(ii) The number of reconstructed events adds up to less than 1,200 events [55–58, 61]. The combined statistical and systematic uncertainties of the parameter $\gamma \equiv F_A/F_V$

extracted by the individual experiments range from 12 % [57] to 56 % [61]. The world average [67]

$$F_A^{\text{pre-2000}} = 0.0116 \pm 0.0016\,, \tag{13}$$

was assigned the confidence level of 0.175 by the PDG.

(iii) There were only two, relatively low precision measurements of F_V resulting in a world average with a 50% uncertainty:

$$F_V^{\text{pre-2000}} = 0.017 \pm 0.008\,, \tag{14}$$

(iv) There was only one, low precision measurement of the $\pi \to e\nu\gamma$ branching fraction, defined over a correlated kinematic region given in equation (10).

(v) The Protvino experiment [61] raised the possibility of a substantial tensor term, F_T, subsequently discussed during more than a decade in a series of theoretical papers [68].

3.3. PIBETA measurements of the $\pi^+ \to e^+\nu_e\gamma$ decay

Study of the radiative pion decay has been a major component in the long term program of the PIBETA/PEN experiments at PSI. Firstly, the strong intrinsic physics significance for low-energy QCD and ChPT as well as the sensitivity to non-$V-A$ interaction terms such as tensor, and its relatively poor experimental quantification prior to 2000 discussed in the preceding section, clearly placed radiative pion decay at high priority. Secondly, $\pi^+ \to e^+\nu\gamma$ events for which the positron annihilates externally create a significant background in the measurement of the pion beta decay $\pi^+ \to \pi^0 e^+\nu$, π_{e3}, the primary goal of the PIBETA experiment, discussed in section 4 below. Thirdly, π_{e3} events for which one of the photons in the subsequent π^0 decay converts into an asymmetric e^+e^- pair, with only one detected electromagnetic shower, create a background for the $\pi_{e2\gamma}$ process. Furthermore, a precise measurement of $R^{\pi}_{e/\mu}$ of equation (2) is impossible without a precise knowledge of the radiative decay width. In fact, because of the overlapping nature of the instrumental response functions to the various decay processes, precision measurement of any one of them requires simultaneous detection and characterization of all pion and muon decay processes present in the data sample.

For all these reasons, the PIBETA collaboration [69] performed a series of measurements at the Paul Scherrer Institute, focused on improving the experimental precision of the $\pi_{e2\gamma}$ branching ratio as well as the form factors F_A and F_V. The apparatus is essentially the same as in the PEN configuration shown in figure 3. The only differences were the absence of the beam mini time projection chamber (mTPC), the use of a segmented target in the early runs (section 4), a thicker active target and degrader detectors to accommodate the higher momentum of $\sim$114 MeV/c, pion beam, and custom electronics for 1- and 2-arm triggers. The arrangement of the central detectors is shown in figure 11. The data were collected in two distinct sets of runs.

The first PIBETA radiative pion decay measuring period took place during 1999–2001, in a configuration optimized for recording pion beta decay, $\pi^+ \to \pi^0 e^+\nu_e$, events

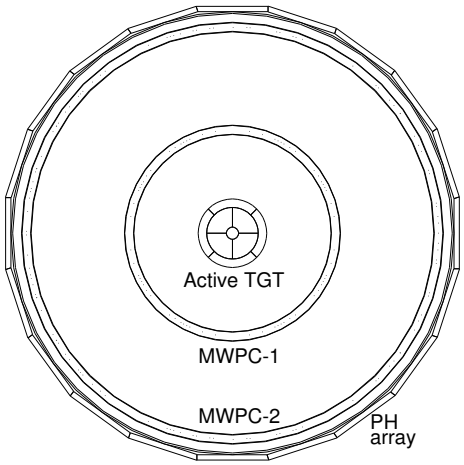

Figure 11. Axial (beam) view of the central detector region during the first PIBETA running period, 1999-2001, and the first half of the 2004 run. Going outward from center we first note the 9-element active target (AT), followed by multiwire proportional chambers MWPC1 and MWPC2, a thin carbon-fiber mechanical shield, and, finally, the 20-element plastic hodoscope (PH). The circumscribed radius is approximately 15 cm.

with a high stopping rate of pions in the target, averaging approximately $8 \times 10^5\,\mathrm{s}^{-1}$. The experiment trigger logic was based on shower energy summed over a cluster of adjacent CsI calorimeter detector modules, with two energy thresholds: a high one of $\sim 51\,\mathrm{MeV}$, and a low one of $\sim 5\,\mathrm{MeV}$. The experiment recorded every event containing two showers, both with energy above the high threshold (HT), and spatially separated by an opening angle $\theta_{12} \gtrsim 90^\circ$. Two-shower events with one exceeding the high and the other the low energy threshold were prescaled by a factor of at least an order of magnitude, while events with two low-threshold showers were prescaled even more. One-arm events, consisting of one shower were also recorded, with the purpose of collecting significant samples of $\pi^+ \to e^+\nu$ and $\mu^+ \to e^+\nu\bar{\nu}$ events for normalization and systematic studies. Detector response to the $\pi \to e\nu$ single-arm events, shown in figure 12, best illustrates the intrinsic performance of the spectrometer. Over 4×10^4 $\pi_{e2\gamma}$ events were collected and analyzed in this set of runs. The results, bringing about an order of magnitude improvement in precision of the branching ratio and F_A/F_V, were published in [40]. However, the authors found a deficit of events in one kinematic region, corresponding to high-E_γ and low-E_e events, that was well outside the limits of the statistical uncertainties of the fit. The authors concluded that further study was needed in a dedicated measurement, as the first run had been optimized for measurement of $\pi^+ \to \pi^0 e^+ \nu_e$ decays.

The second run, dedicated to radiative $\pi_{e2\gamma}$ decays took place in 2004, with the pion stopping rate lowered to $1.5 \times 10^5\,\mathrm{s}^{-1}$ and the trigger electronics modified to accept all high-threshold one-arm events. The first half of the run was carried out with the same detectors as in 1999-2001, while in the second half the 9-element active target was replaced with a single unit. Approximately 2.4×10^4 additional events were collected

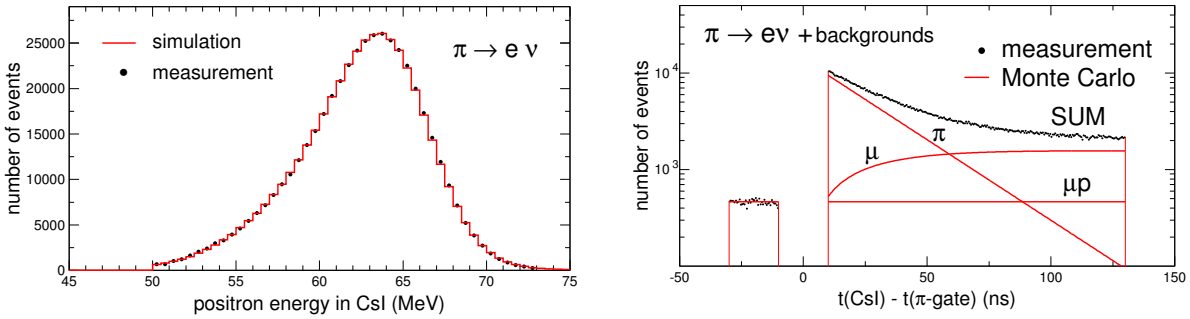

Figure 12. CsI calorimeter response for $\pi \to e\nu$ decays used for calibration and normalization in the PIBETA experiment. Left panel shows the net, background-subtracted energy response for high-threshold events. Energies below $\sim 50\,\mathrm{MeV}$ were dominated by the Michel $\mu^+ \to e^+\nu\bar{\nu}$ decays, and are not shown. The red histogram depicts results of a realistic GEANT3 Monte Carlo simulation. Right panel shows the time response for single-arm high threshold events including backgrounds. Time $t = 0$ is determined by the pion stop; data taking was stopped for approximately 10 ns around the pion stop time (events during this "PROMPT" gate were collected with a high prescaling factor). The main backgrounds come from muon decay, either causal (μ) through the $\pi \to \mu \to e$ decay chain, or acausal (μp) from muons piled-up in the target region. The latter were determined precisely through event triggers for which the decay positron preceded the pion stop signal by up to $\sim 30\,\mathrm{ns}$.

over significantly broader kinematic regions. Most importantly, the lower beam rate resulted in large improvements in the ratio of peak signal to accidental background (P/B) in $\Delta t_{e\gamma}$ spectra, and sufficient low-energy data to perform an independent energy calibration for the charged and neutral showers in the HT trigger. The combined data sets were carefully analyzed, and the results published in [41]. The key results are shown in figures 13, 14 and 15.

With the improved calibrations, the previously observed event deficit vanished, as seen in figure 13, which shows the measured yield in 8 different kinematic regions, compared with the best-fit standard description of equation (7) with the addition of radiative corrections by Bystritsky *et al* [70]. No statistically significant deviations were observed.

The wider kinematic coverage of the new measurement enabled a much improved analysis, including an independent determination of the polar- and axial-vector form factors F_V and F_A, and, for the first time, a determination of the 4-momentum transfer $q^2 = (p_e + p_\nu)^2$ dependence of the polar vector amplitude F_V, figure 14:

$$F_V(q^2) = F_V(0) + aq^2 \qquad \text{with} \qquad a = 0.10 \pm 0.06\,. \tag{15}$$

The uncertainties on the slope parameter are wide enough to accommodate the resonance chiral perturbation calculation of Mateu and Portolés [71].

Even after the inclusion of the lower-energy phase space regions, the PIBETA $\pi_{e2\gamma}$ decay data are strongly dominated by the SD^+ amplitude, leading to a stringent constraint on $F_V + F_A$, and a lax one on $F_V - F_A$. As in previous measurements, the probability of the negative solution for $\gamma = F_A/F_V$ is disfavored by a large factor, about

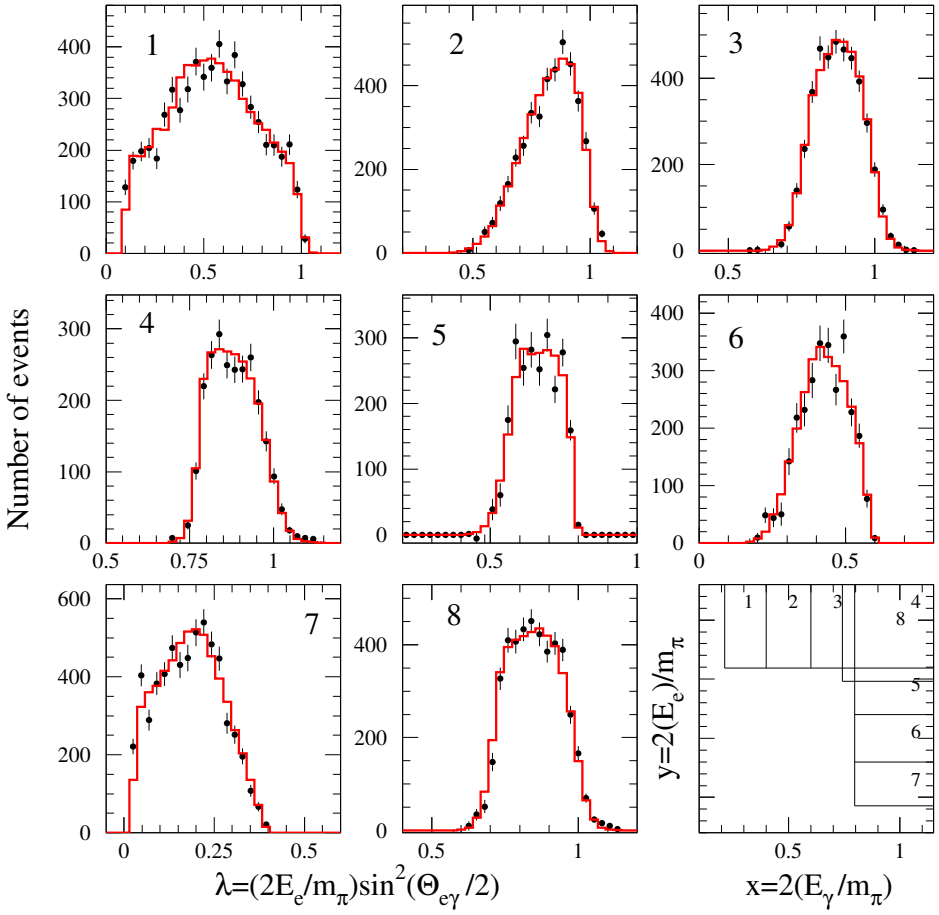

Figure 13. PIBETA data points: background-subtracted $\pi^+ \to e^+\nu_e\gamma$ distribution of the kinematic variable $\lambda \equiv (2E_e/m_\pi)\sin^2(\theta_{e\gamma}/2)$ for 8 regions in the E_e-E_γ (or y-x) plane. The layout of the regions in the x-y plane is indicated in the lower right panel. Solid red histograms: results of GEANT3 calculations for the best-fit values of F_V, F_A, and a.

880. The narrow elliptically shaped locus of best-fit values for F_A and F_V is shown in figure 15. The corresponding equation of the major axis of the ellipse is given by

$$F_A = (-1.0286 \cdot F_V + 0.03853) \pm 0.00014\,. \tag{16}$$

We note that, for a fixed value of F_V, the uncertainty in F_A has been reduced 16-fold compared to the prior world average. In a fully unconstrained fit, the authors report

$$F_V = 0.0258 \pm 0.0017 \qquad \text{and} \qquad F_A = 0.0117 \pm 0.0017\,. \tag{17}$$

The PIBETA result for F_V represents a 5-fold improvement over the prior average. The correlated nature of the PIBETA form factor results allows for a posteriori improvement in precision of F_A as the precision of the determination of the π^0 lifetime improves.

Finally, thanks to the experiment's broad kinematic coverage, the PIBETA authors have reported a branching ratio

$$B_{\pi_{e2\gamma}}(E_\gamma > 10\,\text{MeV}, \theta_{e\gamma} > 40^\circ) = 73.86(54) \times 10^{-8}\,, \tag{18}$$

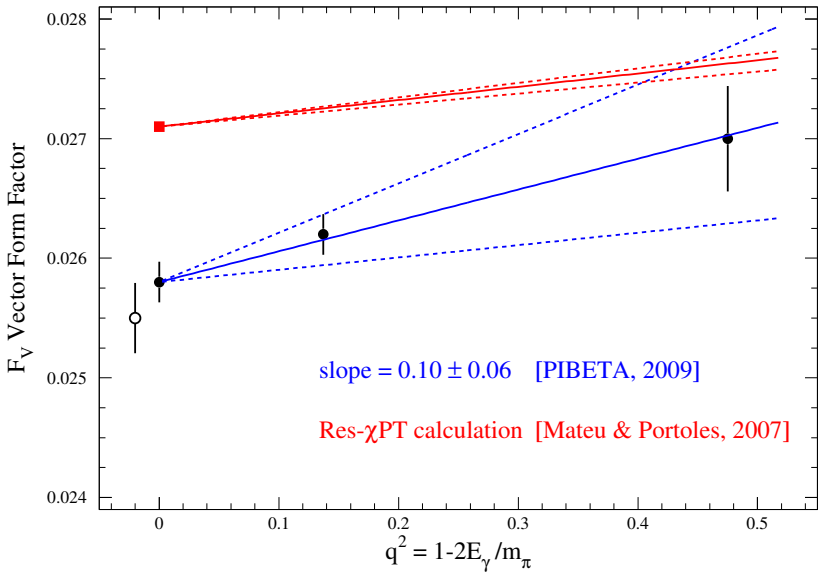

Figure 14. Details of the $q^2 = (p_e + p_\nu)^2$ slope analysis for $F_V(q^2)$ in the PIBETA $\pi_{e2\gamma}$ measurement [41]. Black data points: best-fit values of $F_V(q^2)$ for three momentum bins in the measurement. Solid and dashed blue lines represent the central values and 1σ band, respectively, of the minimum χ^2 fit. Solid red square point and red lines: results of the resonance ChPT calculation of Mateu and Portolés [71]. The current isospin-corrected CVC prediction $F_V(0) = 0.0255 \pm 0.0003$ is indicated by the empty circle offset slightly to $q^2 < 0$ for better visibility.

with more than an order of magnitude improved precision over the previous result.

3.4. Prospects for improvement

The PEN experiment will add new data to the existing $\pi_{e2\gamma}$ data set. Since the PEN beam stopping rate is significantly lower than that used in the 2004 PIBETA run, the impact on the statistical uncertainties will not be great. However, the cleaner running conditions of PEN present greater access to the kinematic region $E_\gamma, E_e < 50\,\text{MeV}$, previously strongly contaminated by muon decay background, and, thus, holding the prospect for a better constraint of the SD^- amplitude, which, in turn, would lead to improved precision in the direct determination of F_V. These results will be forthcoming in the near future.

4. Pion beta decay: $\pi^+ \to \pi^0 e^+ \nu$ (π_{e3})

4.1. General considerations: quark-lepton universality

Unlike the $\pi_{e2(\gamma)}$ decays discussed in the preceding sections, the extremely rare, $\mathcal{O}(10^{-8})$, pion beta decay is not suppressed by any factor apart from the restricted phase space of final states due to the small difference between the charged and neutral pion masses, $\Delta = m_\pm - m_0$. As a pure vector $0^- \to 0^-$ transition, it is completely analogous

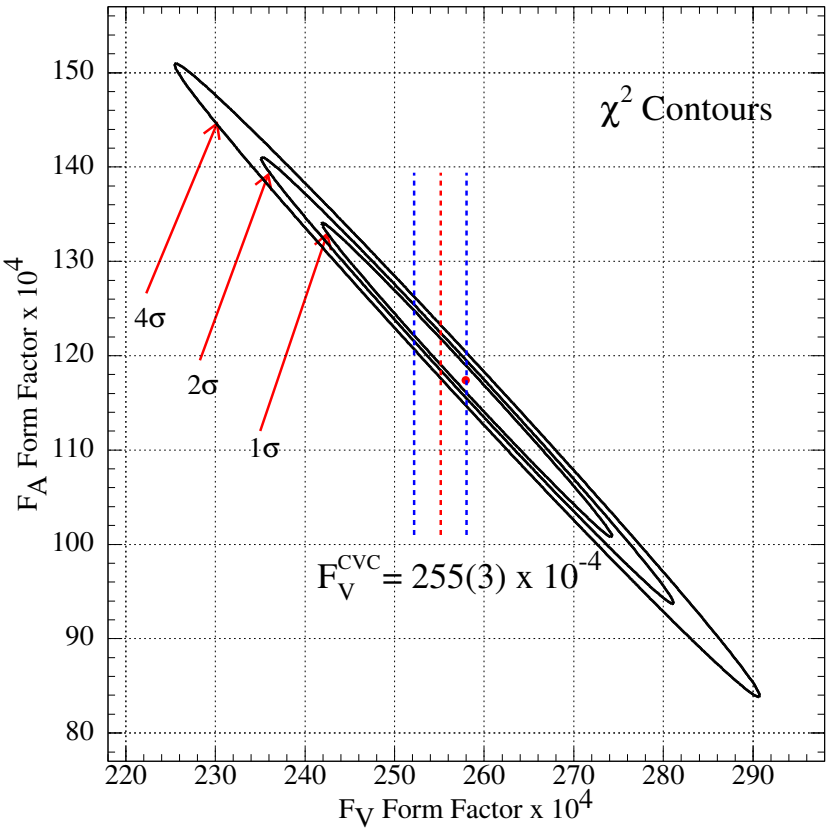

Figure 15. Contour plot of loci of constant χ^2 for the minimum value χ^2_0 (solid red dot) plus 1, 2, and 4 units, respectively, in the $F_A - F_V$ parameter plane, keeping the slope parameter a fixed at the theoretical value $a = 0.041$ [71]. The range of the CVC prediction $F_V = 0.0255 \pm 0.0003$ is indicated by the dashed vertical lines.

to the superallowed Fermi nuclear beta decays. In fact, it can be regarded as the simplest realization of the latter, fully free of complications arising from nuclear structure corrections. Superallowed Fermi decays have historically led to the formulation of the conserved vector current hypothesis, and have played a critical role in testing the unitarity of the Cabibbo-Kobayashi-Maskawa quark mixing matrix through evaluations of the V_{ud} element [72–74].

Within the framework of the $V-A$ theory of the weak interactions, the pion beta decay rate can be expressed in terms of the leading-order width Γ_0 and the radiative and loop corrections δ_π as [75, 76]

$$\Gamma = \Gamma_0(1+\delta_\pi) = \frac{G_F^2|V_{ud}|^2}{30\pi^3}\Delta^5 f(\epsilon,\Delta)\left(1-\frac{\Delta}{2m_+}\right)^3(1+\delta_\pi)\,, \tag{19}$$

where G_F is the Fermi coupling constant and $\epsilon = m_e^2/\Delta^2 \simeq 0.012375$. Finally, up to leading order in $\Delta^2/(m_+ + m_0)^2 \simeq 2.8 \times 10^{-4}$, the function $f(\epsilon,\Delta)$ has the value of $f(\epsilon,\Delta) \simeq 0.94104$. The overall uncertainty of the rate in (19) is dominated by two comparable contributions, one from the Δ^5 factor, and the other from the δ_π radiative/loop corrections, each uncertainty contribution being in the range of 0.05–0.1% of the full rate [37, 73, 77, 78]. Thus, the pion beta decay rate provides a direct means

to determine the CKM matrix element $|V_{ud}|$. In fact, being free of nuclear structure corrections present in superallowed nuclear beta decays, and free of tree-level axial corrections present in neutron beta decay, π_{e3} decay offers the theoretically cleanest path to measuring V_{ud} and, hence, testing quark-lepton universality. However, the extremely low branching ratio for the process has so far limited the experimental accuracy.

Experimentally, $\pi^+ \to \pi^0 e^+ \nu_e$ decay is observed primarily through detection of the final decay particles produced in the near-instantaneous neutral pion decay ($\tau \simeq 8.5 \times 10^{-17}\,\mathrm{s}$). The positron is generally harder to detect with precise efficiency, except for π^+ decays in flight, since its kinetic energy ranges from 0 to only 4 MeV. The key π^0 decay modes and their branching ratios are:

$$\begin{aligned} \pi^0 \to \gamma\gamma\,, \qquad & B \simeq 0.988\,, \\ \gamma e^+ e^-\,, \quad & B \simeq 0.012\,. \end{aligned} \tag{20}$$

All experiments to date have focused on the 2γ channel rather than the $\gamma e^+ e^-$, Dalitz mode. Due to the small charged to neutral pion mass difference, the maximum kinetic energy of the π^0 is low, about 75 keV. Thanks to the correspondingly low π^0 velocity, the directions of the two emitted photons deviate from 180° by no more than 3.8°, on average by $\sim 3.2°$. Furthermore, the Doppler broadening of the photon energies results in a narrow boxlike spectrum between ~ 65.6 MeV and ~ 69.4 MeV. This kinematics provides a robust signal that is additionally separated in time from the dominant prompt hadronic background events thanks to the 26 ns pion lifetime.

4.2. Early measurements

The first observation [79] of the decay at CERN in 1962 using a stopped π^+ beam and a combination of lead glass and NaI(Tl) detectors, was followed by a quick succession of early measurements at CERN [80], Dubna (total absorption Pb glass Čerenkov counters) [81], Columbia University [82], Lawrence Berkeley Lab [83] and Carnegie Tech (now Carnegie Mellon) [84]. The Berkeley, Columbia and Carnegie Tech experiments used combinations of spark chambers and scintillation detectors. The five measurements achieved approximately 20% uncertainties on the branching ratio, based on samples of between 30 and 50 events each.

To date only three measurements of the $\pi^+ \to \pi^0 e^+ \nu_e$ decay branching ratio have been made with precision better than 10%, approximately one for every 20 years, which reflects the challenges of the task.

The CERN group of Depommier *et al* [85] was first to break the 10% uncertainty level in 1967, using a lead glass Čerenkov detector array along with plastic scintillator detectors, as shown in figure 16. The CERN apparatus had an acceptance of $\sim 22.4\%$, and enabled the experimenters to record $332 \pm 10_{\mathrm{bgd}} \pm 23_{\mathrm{stat}}$ pion beta decays from $\sim 1.5 \times 10^{11}$ pion stops in the target. The reported branching ratio value was

$$B(\pi_{e3}) \equiv \frac{\Gamma(\pi^+ \to \pi^0 e^+ \nu)}{\Gamma(\pi^+ \to \mu^+ \nu)} = \left(1.00\,^{+0.08}_{-0.10}\right) \times 10^{-8}\,, \tag{21}$$

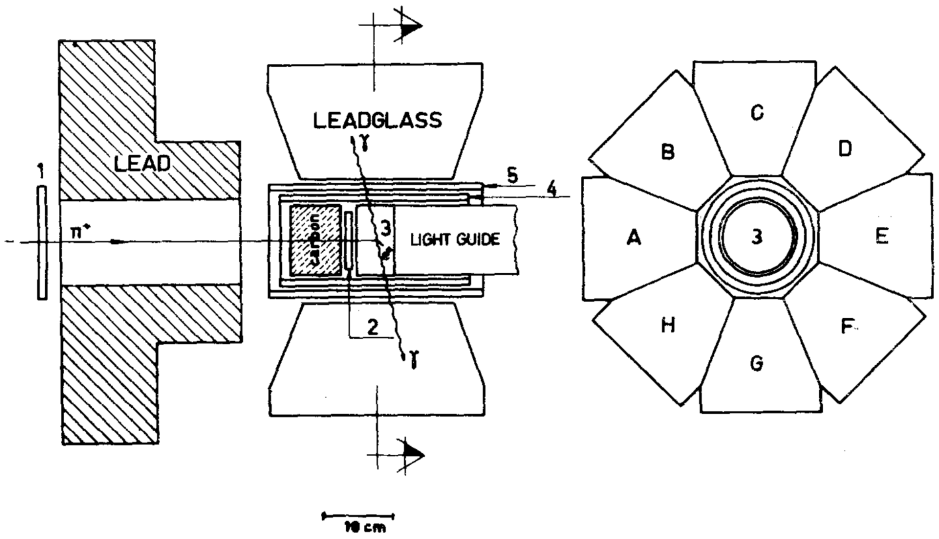

Figure 16. Schematic representation of the CERN pion beta decay apparatus of Depommier *et al* used in their 1967 measurement [85]. Plastic scintillator detectors 1, 2 and 3 define a beam π^+ stop. Candidate pion beta decay events are recorded as narrow coincidences of a pair of electromagnetic showers in the lead glass detectors A through H, delayed with respect to the π^+ stop pulse. Detectors 4 and 5 veto charged particle events in the calorimeter array. For details see [85].

in very good agreement with CVC theory predictions, but not precise enough to test the radiative corrections at $\sim 4\%$. The authors increased the lower-side uncertainty of their result in order to account for the possible influence of nuclear reaction products in their measurement of the π^0 detection efficiency of the lead glass detector array.

In the early 1980's a Temple–Los Alamos group performed a radically different measurement of the pion beta decay rate at the Los Alamos Meson Physics Facility (LAMPF) [86]. Unlike previous experiments which detected decays of π^+'s brought to rest in a target, McFarlane and collaborators detected decays of an intense pion beam in flight in the apparatus shown in figure 17. At 2×10^8 pions/s and with a momentum of $522.1 \pm 0.8\,\mathrm{MeV}/c$, the LAMPF pion beam was orders of magnitude more intense and an order of magnitude higher in energy than in the previous experiments. The decay volume was evacuated to $\sim 10^{-7}$ torr in order to limit the pion hadronic interactions with material in the path, primarily single charge exchange reactions which would be hard to distinguish from pion beta decay events. Because of the low recoil in the π^+ rest frame, the π^0 had transverse momentum of less than $5\,\mathrm{MeV}/c$, or 1% of the longitudinal momentum. The average π^0 momentum of about $505\,\mathrm{MeV}/c$ implied a short mean π^0 laboratory flight length of about 100 nm before decay. The acceptance was defined by the combination of an upstream collimator, minimum opening angle of the two photons, and the solid angle of the active area of the two photon detectors. The latter were the two arms of the LAMPF π^0 spectrometer [87], appropriately modified [86] for the pion beta decay measurement. Each photon detector arm consisted of a front plastic scintillator veto detector followed by three successive lead glass converter layers (0.56 radiation

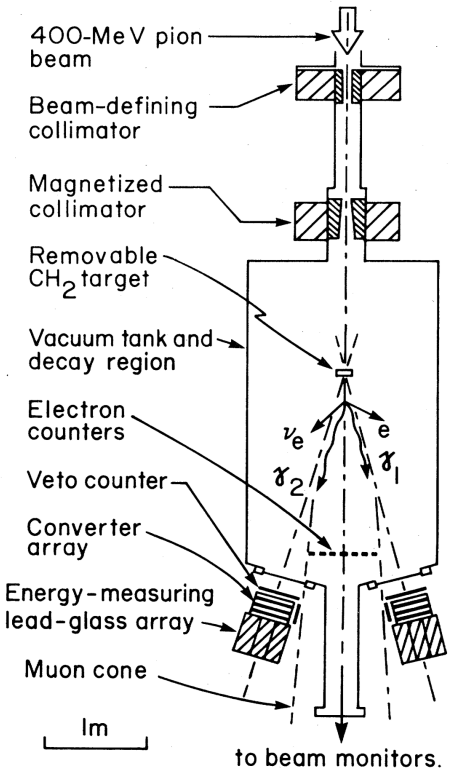

Figure 17. Schematic representation of the Temple–Los Alamos pion beta decay apparatus that McFarlane *et al* used in their 1984 measurement [86]. The removable CH_2 target was used for calibrations and removed during decay measurements. For further details see [86].

length thick, each). Each converter layer was followed by two scintillation hodoscopes for position and time measurement. Finally, behind the forward crate containing the converter-hodoscope layers was a rear crate with an array of 15 lead glass blocks, forming a 14 radiation lengths thick calorimeter. The cross sectional area of the detector package as seen by the photons was 45 cm × 75 cm. The arms were well matched to detecting the final-state photons that ranged between 175 and 350 MeV in energy. At $\sigma_t \simeq 250$ ps per arm, the time resolution was excellent for such large detectors. At $\sigma_E \simeq 1.53\sqrt{E}$ (in MeV), the energy resolution was adequate for the task.

This measurement apparatus has several advantages over the stopped decay technique. First, the hadronic background can be effectively eliminated in an evacuated decay region. Second, the high pion beam momentum focuses the decay photons into a solid angle significantly smaller than 4π sr. Finally, in principle, the measurement can be done with both charged pion states, although in practice the intensity of π^- beams is significantly lower than that of π^+.

However, there are also significant disadvantages compared to the stopped decay measurement. The proper time that beam pions spend in the decay region is very short, about 10^{-3} pion lifetimes, requiring enormously higher beam intensities to achieve high statistical precision for the rare pion beta decays. Normalization, i.e.,

counting the number of pions passing through the apparatus is very challenging, as the readily available processes such as the $\pi_{\mu 2}$ decay have radically different kinematics and detection systematics, and require separate detectors. Finally, detection efficiency (including detector acceptance), as well as trigger and event selection efficiency must be determined in absolute terms with high precision.

Given all the above considerations, the Temple–LAMPF group reported the experimental partial rate, $1/\tau_{\pi\beta}$, and branching ratio, $B_{\pi\beta}$:

$$\frac{1}{\tau_{\pi\beta}} = (0.394 \pm 0.015)\,\mathrm{s}^{-1} \qquad \text{or} \qquad B_{\pi\beta} = (1.026 \pm 0.039) \times 10^{-8}\,, \quad (22)$$

based on 1124 ± 36 pion beta decay events, and 2.14×10^{14} beam pions. The overall 3.8% uncertainty breaks down to 3.1% statistical and 2.0% systematic contributions. The largest systematic uncertainty contributions arose from the number of beam pions, time in decay region, and the various efficiencies. The authors also extracted a new value of 0.964 ± 0.019 for the cosine of the Cabibbo angle, or V_{ud}. While not as precise as the contemporary values of V_{ud} derived from superallowed Fermi nuclear beta decays, it was consistent with them.

4.3. The PIBETA experiment

The primary goal of the PIBETA experiment conducted at PSI and introduced in sections 2 and 3, was to improve by an order of magnitude the existing experimental precision of the pion beta decay branching ratio. The apparatus is described schematically in figure 3, while the central detector region is shown in figure 11. A $\sim$114 MeV/c pion beam of the PSI πE1 beamline was focused onto the segmented nine-element active target which stopped an average of $0.8 - 1 \times 10^6$ pions/s. The PIBETA approach was essentially similar to the 1967 CERN experiment of Depommier *et al* [85], but with larger acceptance, much improved energy resolution of the electromagnetic shower calorimeter, MWPC tracking of charged particles between the central region and the calorimeter, a more intense pion beam, and faster electronics and data acquisition system. The key detector response functions to pion beta decay events are shown in figures 18, 19 and 20. The corresponding spectra for the normalizing π_{e2} decay, and for the $\pi_{e2\gamma}$ decay which can contribute background events for the pion beta decay, are shown in sections 2.3 and 3.3. Since a subset of pion beta decays can also be misidentified as radiative $\pi_{e2\gamma}$ decays, it was essential that all three processes be simultaneously accounted for and understood at the few parts per thousand level. In fact, ordinary ("Michel") and radiative muon decays, though not discussed here, were included as well in the comprehensive PIBETA analysis, since they comprise the majority of actual events occurring in the apparatus, and dominate the accidental background to all pion decay channels. Figures 18 – 20 demonstrate that the pion beta decay event sample was clean and well described in terms of the relevant instrumental resolutions.

During three runs in 1999, 2000 and 2001, the PIBETA collaboration acquired over 64,000 pion beta decay events, which led to an improvement of the experimental

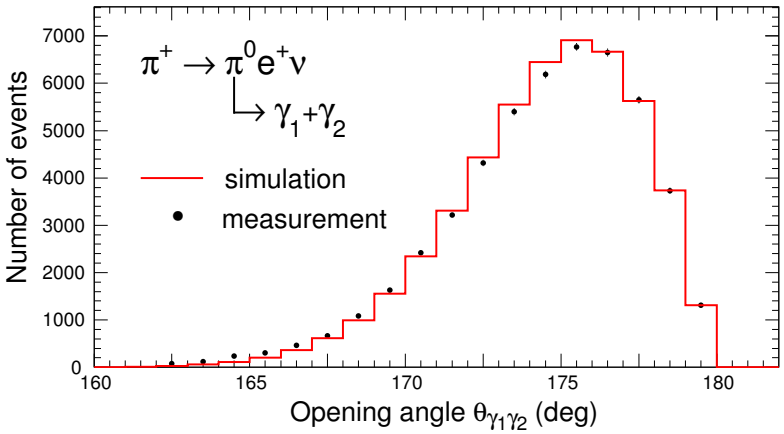

Figure 18. Distribution of $\gamma_1 - \gamma_2$ photon opening angle in the PIBETA experiment for the pion beta decay event sample. Data points reflect measurements, while the red histogram indicates results of a realistic GEANT3 Monte Carlo simulation including the full effects of the PIBETA detector resolution. Radiative $\pi_{e2\gamma}$ decay events, if misidentified as π_{e3} events through positron annihilation in flight, have a significantly different $\theta_{\gamma 1 \gamma 2}$ signature.

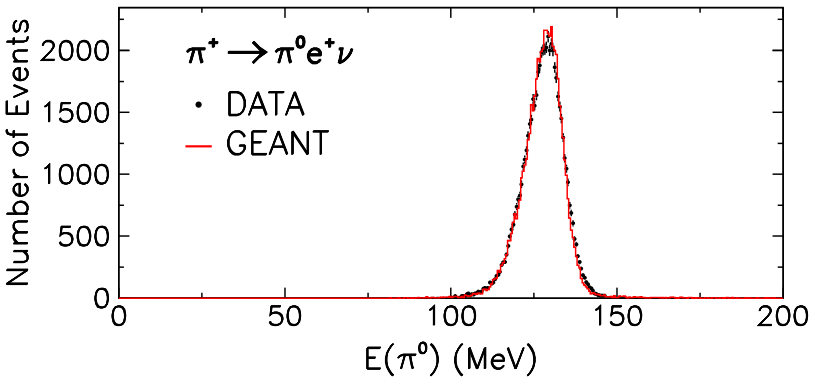

Figure 19. Distribution of the π^0 energy in the PIBETA experiment. Data points reflect measurements, while the red histogram indicates results of a realistic GEANT3 Monte Carlo simulation including the full effects of the PIBETA detector resolution.

precision of the π_{e3} branching ratio of about an order of magnitude [39]. The PIBETA result was evaluated in two ways, (a) normalizing to the average experimental π_{e2} branching ratio of (5) $R^{\pi}_{e/\mu} = (1.230 \pm 0.004) \times 10^{-4}$ ("exp. norm."), and (b) normalizing to the established theoretical value of (3), $R^{\pi}_{e/\mu} = (1.2352 \pm 0.0005) \times 10^{-4}$ ("theo. norm."). The resulting values were:

$$B^{\text{exp. norm.}}_{\pi\beta} = [1.036 \pm 0.004(\text{stat}) \pm 0.004(\text{syst}) \pm 0.003(\pi_{e2})] \times 10^{-8}, \quad (23)$$

$$B^{\text{theo. norm.}}_{\pi\beta} = [1.040 \pm 0.004(\text{stat}) \pm 0.004(\text{syst})] \times 10^{-8}\,. \quad (24)$$

The external experimental uncertainty included the branching ratios $R^{\pi\ \text{exp}}_{e/\mu}$, $B^{\text{exp}}_{\pi^0 \to \gamma\gamma}$ and that of $\tau^{\text{exp}}_{\pi^+}$, the pion lifetime, and were dominated by the former. The combined internal systematic uncertainty was dominated by the uncertainties related to the ratio of the "pion gate" live fractions for the π_{e3} and π_{e2} processes, and the number of the

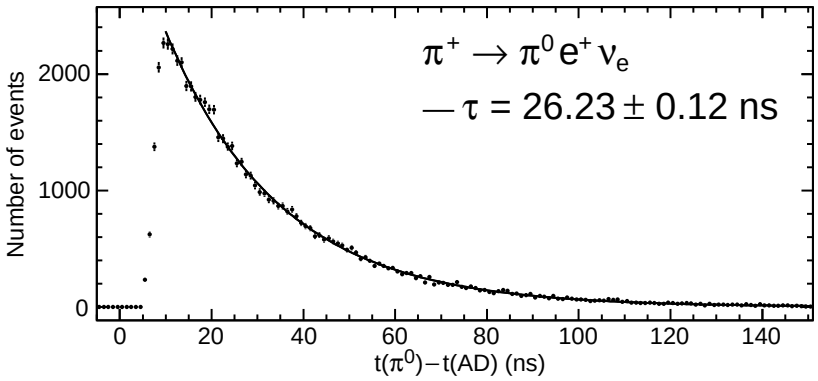

Figure 20. Distribution of the π^0 event times with respect to the time $t = 0$ of the active degrader (AD) signal, reflecting the beam pion stop time, in the PIBETA experiment. The curve is a best-fit exponential decay with the decay parameter in good agreement with 26.03 ns, the pion lifetime. The time range of ± 5 ns around $t = 0$, the pion stop time, was vetoed in the decay event trigger in order to suppress prompt hadronic backgrounds which had a $\sim 10^4$ times higher rate than the π_{e3} events. A prescaled sample of the prompt hadronic events was collected for systematic studies and calibrations.

π_{e2} events used for normalization, followed by the ratio of acceptances for the same two processes.

This result represents the most stringent test of CVC and Cabibbo universality in a meson, as well as of the proper treatment of the radiative corrections, which, combined, predict $B^{\rm SM}_{\pi\beta} = (1.038 - 1.040) \times 10^{-8}$ at 90% confidence limits [67]. Excluding radiative corrections gives the range $B^{\rm SM}_{\pi\beta} = (1.005 - 1.007) \times 10^{-8}$, a $> 4\sigma$ discrepancy from the PIBETA result. The PIBETA collaborators also extracted

$$V_{ud}^{\pi\beta/\text{exp. norm.}} = 0.9728 \pm 0.0030\,, \text{ and} \tag{25}$$

$$V_{ud}^{\pi\beta/\text{theo. norm.}} = 0.9748 \pm 0.0025\,. \tag{26}$$

These values are in excellent agreement with the PDG recommended value for V_{ud}, although five times less precise.

Following in the same vein, it is tempting to go one step further and turn the PIBETA determination of the π_{e3} branching ratio around, using it instead to evaluate $R^{\pi}_{e/\mu}$. This is accomplished by fixing V_{ud} to its extraordinarily precise PDG 2013 recommended value of 0.97425 ± 0.00022 and adjusting $R^{\pi}_{e/\mu}$ until the extracted value of $V^{\pi\beta}_{ud}$ agrees. This intriguing exercise yields

$$(R^{\pi}_{e/\mu})^{\rm PIBETA} = (1.2366 \pm 0.0064) \times 10^{-4}\,, \tag{27}$$

in good agreement with direct measurements reviewed in section 2. Appropriately averaging this value of $R^{\pi}_{e/\mu}$ with those listed in table 1, one obtains a slightly higher value than the current PDG average: $(R^{\pi}_{e/\mu})^{\text{new avg}} = (1.2317 \pm 0.0031) \times 10^{-4}$.

Given the advantage in lower theoretical uncertainties compared to nuclear decays, there was every incentive to pursue a higher precision result in the pion beta decay rate or branching ratio. However, the urgency of a further improvement was considerably

reduced by the Brookhaven National Laboratory experiment BNL E865 result [88] and the subsequent renormalization of V_{us} that removed a longstanding 2–3σ shortfall in CKM matrix unitarity. In light of the considerable experimental challenges that an improved measurement would pose, the present full agreement of available data on V_{ud} with CKM unitarity means that a major new project on improving the precision of pion beta decay is not currently planned. We note, though, that the status of neutron beta decay is in considerable flux, with major discrepancies in the available data sets on both the beta asymmetry and the neutron lifetime [89, 90]. At present there are a number of projects addressing these deficiencies. While not as theoretically clean as the pion beta decay, neutron decay is free of the nuclear structure and Coulomb corrections that affect nuclear beta decays, including the superallowed Fermi $0^+ \to 0^+$ transitions [91].

5. Summary

A close look at the recent record of study of the decays of the charged pion reveals a great deal of activity and continued strong relevance. The extraordinary precision of the theoretical description of the π_{l2}, $\pi_{l2\gamma}$, $\pi_{l2e^+e^-}$ and π_{e3} decays remains unmatched by the available experimental results. There have been impressive advances in the precision of the π_{e3} and $\pi_{e2\gamma}$ decays in the past decade. As of this writing, we are on the verge of a significant improvement of the π_{e2} decay precision, as the PEN and PiENu experiments complete their analyses. Even subsequent to that development, there will remain considerable room for improvement of experimental precision with high payoff in terms of limits on physics not included in the present Standard Model. This work remains relevant and complementary to the direct searches on the energy frontier currently under way at particle colliders, with considerable theoretical significance.

Acknowledgments

This work has been supported by grants from the US National Science Foundation (most recently PHY-1307328) and the Paul Scherrer Institute.

References

[1] Lattes C M G, Muirhead H, Occhialini G P S and Powell C F 1947 *Nature* **159** 694
[2] Ruderman M A and Finkelstein R J 1949 *Phys. Rev.* **76** 1458
[3] Feynman R P and Gell-Mann M 1958 *Phys. Rev.* **109** 193
[4] Gershtein S S and Zeldovich Y B *Zh. Eksp. Teor. Fiz.* **29** 698; [*Sov. Phys. JETP* **2** 576 (1957)]
[5] Fazzini T, Fidecaro G, Merrison A W, Paul H and Tollestrup A V 1959 *Phys. Rev. Lett.* **1** 247
[6] Impeduglia G *et al* 1959 *Phys. Rev. Lett.* **1** 249
[7] Anderson H L, Fujii T, Miller R H and Tau L 1959 *Phys. Rev. Lett.* **2** 53
[8] S. M. Berman 1958 *Phys. Rev. Lett.* **1** 468
[9] Kinoshita T 1959 *Phys. Rev. Lett.* **2** 477
[10] Anderson H L, Fujii T, Miller R H and Tau L 1960 *Phys. Rev.* **119** 2050
[11] Di Capua E, Garland R, Pondrom L and Strelzoff A 1964 *Phys. Rev.* **133** B1333

[12] Goldstone J 1961 *Nuovo Cimento* **19** 154
[13] Goldstone J, Salam A and Weinberg S 1962 *Phys. Rev.* **127** 965
[14] Nambu Y and Iona-Lasinio G 1961 *PR* **122** 345
[15] Gell-Mann M, Oakes R and Renner B 1968 *Phys. Rev.* **175** 2195
[16] Weinberg S 1979 *Physica* **96A** 327
[17] Gasser J and Leutwyler H 1982 *Phys. Reports* **87** 77
[18] Gasser J and Leutwyler H 1984 *Ann. Phys.* **158** 142
[19] For a review, see Pich A 1995 *Rept. Prog. Phys.* **58** 563
[20] For a detailed discussion see, e.g., Donoghue J F, Golowich E and Holstein B R 1992 *Dynamics of the Standard Model* (Cambridge)
[21] For a detailed discussion of the fundamentals of the $\pi_{e2(\gamma)}$ decay see, e.g., Bryman D A, Depommier P and Leroy C 1982 *Phys. Rep.* **88** 151
[22] Marciano W J and Sirlin A 1993 *Phys. Rev. Lett.* **71** 3629
[23] Finkemeier M 1996 *Phys. Lett. B* **387** 391
[24] Cirigliano V and Rosell I 2007 *Phys. Rev. Lett.* **99** 231801
[25] Schrock R E 1981 *Phys. Rev. D* **24**, 5
[26] Shanker O U 1982 *Nucl. Phys.* **B204** 375
[27] Loinaz W, Okamura N, Rayyan S, Takeuchi T, Wijewardhana L C R 2004 *Phys. Rev. D* **70** 113004
[28] Ramsey-Musolf M J Su S and Tulin S 2007 *Phys. Rev. D* **76** 095017
[29] Campbell B A and Maybury D W 2005 *Nucl. Phys.* **B709** 419
[30] Campbell B A and Ismail A 2008 Leptonic Pion Decay And Physics Beyond The Electroweak Standard Model *Preprint* hep-ph/0810.4918
[31] `http://pen.phys.virginia.edu/` and links therein
[32] `http://pienu.triumf.ca/` and links therein
[33] Bryman D, Marciano W J, Tschirhart R and Yamanaka T 2011 *Annu. Rev. Nucl. Part. Sci.* **61** 331
[34] Bryman D A *et al* 1986 *Phys. Rev. D* **33** 1211
[35] Britton D I *et al* 1992 *Phys. Rev. Lett.* **68** 3000; Britton D I *et al* 1992 *Phys. Rev. D* **46** R885
[36] Czapek G *et al* 1993 *Phys. Rev. Lett.* **70** 17
[37] Beringer J *et al* (Particle Data Group) 2012 *Phys. Rev. D* **86** 010001
[38] Frlež E *et al* 2004 *Nucl. Instrum. Methods A* **526** 300
[39] Počanić D *et al* 2004 *Phys. Rev. Lett.* **93** 181803
[40] Frlež E *et al* 2004 *Phys. Rev. Lett.* **93** 181804
[41] Bychkov M *et al* 2009 *Phys. Rev. Lett.* **103** 181803
[42] Počanić D *et al* 2014 New results in rare allowed muon and pion decays *Preprint* nucl-ex/1403.7416
[43] Palladino A 2012 PhD thesis, University of Virginia, and Palladino A, van der Schaaf A and Počanić, to be published
[44] Aguilar-Arevalo A *et al* 2009 *Nucl. Instrum. Methods A* **609** 102
[45] Blanpied G 1996 *et al Phys. Rev. Lett.* **76** 1023
[46] Aguilar-Arevalo A *et al* 2010 *Nucl. Instrum. Methods A* **621** 188
[47] Chiang I H *et al* 1995 *IEEE Trans. Nucl. Sci.* **42** 394
[48] Komatsubara T K *et al* 1998 *Nucl. Instrum. Methods A* **404** 315
[49] Bernstein A M and Holstein B R 2013 *Rev. Mod. Phys.* **85** 49
[50] De Baenst P and Pestieau J 1968 *Nuovo Cimento* **53A** 407
[51] Vaks V G and Ioffe B L 1958 *Nuovo Cimento* **10** 342
[52] Neville D E 1961 *Phys. Rev.* **124** 2037
[53] Muller V F 1963 *Z. Phys.* **173** 438
[54] Larin I *et al* (PrimEx Collaboration) 2011 *Phys. Rev. Lett.* **106** 162303
[55] Depommier P, Heintze J, Rubbia C and Soergel V 1963 *Phys. Lett.* **7** 285
[56] Stetz A *et al* 1978 *Nucl. Phys.* **B137** 285
[57] Bay A *et al* 1986 *Phys. Lett.* **B321** 212

[58] Piilonen L E *et al* 1986 *Phys. Rev. Lett.* **57** 1402
[59] R. D. Bolton R D *et al* 1984 *Phys. Rev. Lett.* **53** 1415
[60] Dominguez C A and Solà J 1988 *Phys. Lett.* **B208** 131
[61] Bolotov V N *et al* 1990 *Phys. Lett.* **B243** 308
[62] Korenchenko S M *et al* 1976 *Sov. Phys.–JETP* **44** 35
[63] Egli S *et al* (SINDRUM Collaboration) 1986 *Phys. Lett.* **B175** 97
[64] Egli S *et al* (SINDRUM Collaboration) 1989 *Phys. Lett.* **B222** 533
[65] Bertl W *et al* (SINDRUM Collaboration) 1985 *Nucl. Phys.* **B260** 1
[66] Baranov V A *et al* 1992 *Sov. J. Nucl. Phys.* **55** 1644 [transl. from *Yad. Fiz.* **55** 2940]
[67] see, e.g., Eidelman S *et al* (Particle Data Group) 2004 *Phys. Lett.* **B592** 1
[68] Poblaguev A A 1990 *Phys. Lett.* **B238** 108; Poblaguev A A 1992 *Phys. Lett.* **B286** 169; Chizhov M V 2005 *Phys. Part. Nucl. Lett.* **2** 193, and references therein
[69] `http://pibeta.phys.virginia.edu/` and links therein
[70] Bystritsky Y M, Kuraev E A and Velicheva E P 2004 *Phys. Rev. D* **69** 114004
[71] Mateu V and Portolés J 2007 *Eur. Phys. J. C* **52** 325
[72] Czarnecki A, Marciano W J and Sirlin A 2004 *Phys. Rev. D* **70** 093006
[73] Marciano W J and Sirlin A 2006 *Phys. Rev. Lett.* **96** 032002
[74] Hardy J C and Towner I S 2009 *Phys. Rev. C* **79** 055502
[75] Källen G K 1964 *Elementary Particle Physics* (Addison-Wesley, Reading, MA), p 400 *et seq*
[76] Sirlin A 1978 *Rev. Mod. Phys.* **50** 573
[77] Cirigliano V, Knecht M, Neufeld H and Pichl H 2003 *Eur. Phys. J. C* **27** 255
[78] Passera M, Phillippides K and Sirlin A 2011, *Phys. Rev. D* **84** 094030
[79] Depommier P, Heintze J, Mukhin A, Rubbia C, Soergel V and Winter K 1962 *Phys. Lett.* **2** 23
[80] Depommier P, Heintze J, Rubbia C and Soergel V 1963 *Phys. Lett.* **5** 61
[81] Dunaitsev A F, Petrukhin V I, Prokoshkin Yu D and Rykalin V I 1964 *JINR report 1559*
[82] Bartlett D, Devons S, Meyer S L and Rosen J L 1964 *Phys. Rev.* **136** B1452
[83] Bacastow R, Chesquière C, Wiegand C and Larsen R R 1965 *Phys. Rev.* **139** B407
[84] Bertram W K, Meyer D I, Carrigan, Jr, R A and Nadelhaft I 1965 *Phys. Rev.* **139** B617
[85] Depommier P, Duclos J, Heintze J, Kleinknecht K, Riesenberg H and Soergel V 1968 *Nucl. Phys.* **B4** 189
[86] McFarlane *et al* 1985 *Phys. Rev. D* **32** 547
[87] Baer H W *et al* 1980 *Nucl. Instrum. Methods* **180** 445
[88] Sher A *et al* 2003 *Phys. Rev. Lett.* **91** 261802
[89] Baeßler S, Bowman J D, Penttilä S and Počanić D 2014 *J. Phys. G: Nucl. Part. Phys.* [in press; this issue]
[90] Young A *et al* 2014 *J. Phys. G: Nucl. Part. Phys.* [in press; this issue]
[91] For details see, e.g., Holstein B R 2014 *J. Phys. G: Nucl. Part. Phys.* [in press; this issue], and references therein